Tran-SET

Transportation Consortium of South-Central States

Solving Emerging Transportation Resiliency, Sustainability, and Economic Challenges through the Use of Innovative Materials and Construction Methods: From Research to Implementation

Advanced Modeling and Design Methodology for Pavements using Plasticity-Based Shakedown Theory

Project No. 19PLSU09

Lead University: Louisiana State University

Final Report

November 2020

Disclaimer

The contents of this report reflect the views of the authors, who are responsible for the facts and the accuracy of the information presented herein. This document is disseminated in the interest of information exchange. The report is funded, partially or entirely, by a grant from the U.S. Department of Transportation's University Transportation Centers Program. However, the U.S. Government assumes no liability for the contents or use thereof.

Acknowledgements

The authors would like to acknowledge the comments and suggestions provided by the following Project Review Committee members: Jeff Lambert; Michael Dunning; and Pravat Karki.

TECHNICAL DOCUMENTATION PAGE

1. Project No.	2. Government Accession No.	3. Recipient's Catalog No.
19PLSU09		

4. Title and Subtitle	5. Report Date
Advanced Modeling and Design Methodology for Pavements using Plasticity-Based Shakedown Theory	Nov. 2020
	6. Performing Organization Code
7. Author(s) PI: Shengli Chen https://orcid.org/0000-0002-5595-8692 Co-PI: Chao Sun https://orcid.org/0000-0003-3909-0325 GRA: Xu Wang https://orcid.org/0000-0002-9012-8395 GRA: Zhiming Zhang https://orcid.org/0000-0002-7678-605X	8. Performing Organization Report No.
9. Performing Organization Name and Address Transportation Consortium of South-Central States (Tran-SET) University Transportation Center for Region 6 3319 Patrick F. Taylor Hall, Louisiana State University, Baton Rouge, LA 70803	10. Work Unit No. (TRAIS)
	11. Contract or Grant No.
12. Sponsoring Agency Name and Address United States of America Department of Transportation Research and Innovative Technology Administration	13. Type of Report and Period Covered Final Research Report August 2019 – November 2020
	14. Sponsoring Agency Code

15. Supplementary Notes

16. Abstract

Pavement design is a process intended to find the most economical combination of layer thickness and material type for the pavement, taking into account the properties of the subgrade soil and the traffic to be carried during the service life of the road. The currently prevalent methods of pavement analysis and design, however, are more or less empirical in U.S., which possess the shortcoming that the important type of pavement distress of rutting related to the accumulation of plastic or permanent deformations cannot be effectively considered. This project proposes an exploratory study on the application of the plasticity theory-based shakedown concept to the analysis and design of pavements under repeated loading, with a more realistic incorporation of the roughness impact of the top pavement layer on the dynamic amplification of vehicle loading as well as on the elastic stress responses in the underlying subsoils. Numerical results from the newly developed vehicle-road coupling model show that the total vehicle load amplification factor ranges from 0.88 to 1.16 under different roughness levels and traveling speeds. This indicates the necessity and importance of incorporating the factors of roughness/vehicle speed in the pavement response analysis. Extensive parametric analyses for the shakedown limit show that increases in the pavement cohesion strength and internal friction angle and in the pavement thickness have a positive influence on the calculated shakedown limit value. The analysis results also indicate that there generally exists an optimal Young's modulus ratio between the pavement and subsoil, for which a maximum shakedown load of the pavement system will be reached. The outcomes of this project on one hand add contributions to the development of a more rational theoretical framework for the pavement design/analysis. On the other hand, the shakedown design approach can prevent the flexible pavement from excessive rutting failure, and hence is of great practical value for prediction/design of the vehicle load, traveling speed, and layer thickness that is required to warrant shakedown state of the pavements (i.e., no excessive rutting) in the long run.

17. Key Words	18. Distribution Statement
Vehicle-road coupling model, multi-layered pavement system, plasticity-based shakedown theorem, lower bound shakedown limit	No restrictions. This document is available through the National Technical Information Service, Springfield, VA 22161.

19. Security Classif. (of this report)	20. Security Classif. (of this page)	21. No. of Pages	22. Price
Unclassified	Unclassified	49	

Form DOT F 1700.7 (8-72) **Reproduction of completed page authorized.**

SI* (MODERN METRIC) CONVERSION FACTORS

APPROXIMATE CONVERSIONS TO SI UNITS

Symbol	When You Know	Multiply By	To Find	Symbol
		LENGTH		
in	inches	25.4	millimeters	mm
ft	feet	0.305	meters	m
yd	yards	0.914	meters	m
mi	miles	1.61	kilometers	km
		AREA		
in^2	square inches	645.2	square millimeters	mm^2
ft^2	square feet	0.093	square meters	m^2
yd^2	square yard	0.836	square meters	m^2
ac	acres	0.405	hectares	ha
mi^2	square miles	2.59	square kilometers	km^2
		VOLUME		
fl oz	fluid ounces	29.57	milliliters	mL
gal	gallons	3.785	liters	L
ft^3	cubic feet	0.028	cubic meters	m^3
yd^3	cubic yards	0.765	cubic meters	m^3
		NOTE: volumes greater than 1000 L shall be shown in m^3		
		MASS		
oz	ounces	28.35	grams	g
lb	pounds	0.454	kilograms	kg
T	short tons (2000 lb)	0.907	megagrams (or "metric ton")	Mg (or "t")
		TEMPERATURE (exact degrees)		
°F	Fahrenheit	5 (F-32)/9 or (F-32)/1.8	Celsius	°C
		ILLUMINATION		
fc	foot-candles	10.76	lux	lx
fl	foot-Lamberts	3.426	$candela/m^2$	cd/m^2
		FORCE and PRESSURE or STRESS		
lbf	poundforce	4.45	newtons	N
lbf/in^2	poundforce per square inch	6.89	kilopascals	kPa

APPROXIMATE CONVERSIONS FROM SI UNITS

Symbol	When You Know	Multiply By	To Find	Symbol
		LENGTH		
mm	millimeters	0.039	inches	in
m	meters	3.28	feet	ft
m	meters	1.09	yards	yd
km	kilometers	0.621	miles	mi
		AREA		
mm^2	square millimeters	0.0016	square inches	in^2
m	square meters	10.764	square feet	ft^2
m	square meters	1.195	square yards	yd^2
ha	hectares	2.47	acres	ac
km	square kilometers	0.386	square miles	mi^2
		VOLUME		
mL	milliliters	0.034	fluid ounces	fl oz
L	liters	0.264	gallons	gal
m	cubic meters	35.314	cubic feet	ft^3
m	cubic meters	1.307	cubic yards	yd^3
		MASS		
g	grams	0.035	ounces	oz
kg	kilograms	2.202	pounds	lb
Mg (or "t")	megagrams (or "metric ton")	1.103	short tons (2000 lb)	T
		TEMPERATURE (exact degrees)		
C	Celsius	1.8C+32	Fahrenheit	°F
		ILLUMINATION		
lx	lux	0.0929	foot-candles	fc
cd/m^2	$candela/m^2$	0.2919	foot-Lamberts	fl
		FORCE and PRESSURE or STRESS		
N	newtons	0.225	poundforce	lbf
kPa	kilopascals	0.145	poundforce per square inch	lbf/in^2

TABLE OF CONTENTS

LIST OF FIGURES

LIST OF TABLES

ACRONYMS, ABBREVIATIONS, AND SYMBOLS

AASHO	American Association of State Highway Officials
FIT	Fourier Integral Transform
HMA	Hot Mix Asphalt
IFFT	Inverse Fast Fourier Transform
IRI	International Roughness Index
ISO	International Organization for Standardization
ME	Mechanistic-Empirical
PSD	Power Spectral Density
TRM	Transmission and Reflection Matrix
a, b	half-length of each side of the rectangular contact area
C_v	damping and stiffness matrices
c	material cohesion
c_{ij}	damping matrices
c_R	Rayleigh wave speed
c_s	shear wave speed of soil
c_{s1}, c_{s2}	damping coefficients of the front and rear suspensions, respectively
c_{t1}, c_{t2}	damping coefficients of the front and rear tires, respectively
c_u	tire damping constant
E	Young's modulus
F	generalized force vector
F_v	the force vector
f	the yield criterion of pavement system materials
f_1, f_2, f_3, and f_4	the generalized force vector components corresponding to the four degrees of freedom
$H(\dots)$	the Heaviside function
I_c	half of vehicular body lateral mass moment of inertia
i	the unit imaginary
K_v	stiffness matrices

k_{ij}	elements of the stiffness
k_s	suspension spring constant
k_{s1}, k_{s2}	stiffness coefficients of the front and rear suspensions
k_{t1}, k_{t2}	the stiffness coefficients of the front and rear tires
k_u	tire spring constant
M_v	system mass
m_c	half of vehicular body mass
m_f, m_r	the mass of a front wheel, and the mass of a rear wheel
m_{ij}	the element of the mass matrix
m_s	sprung mass
m_u	unsprung mass
Q_{dyn}	the additional vehicle load induced by road roughness
Q_{sta}	the static load due to self-weight
q	the constant magnitude of the moving load
$S(n_k)$	the power spectrum density function
$S_{\xi}(\kappa_0)$	the PSD at κ_0 or initial PSD
s_1, s_2	the distance of the center of gravity of the vehicular body from the front and rear axles
T	Kinetic energy of the multi-degree freedom vehicle system
t	time
$u_i(i = x, y, z)$	displacements of the pavement/subsoil
$\hat{\tilde{u}}_i\ (i = x, y, z)$	displacement in FIT Domain
V	Potential energy of the multi-degree freedom vehicle system
v	the traveling speed
$\dot{Z}$	the first and second derivatives of Z with respect to time t
$\ddot{Z}$	the second derivatives of Z with respect to time t
Z_c	vertical displacement of vehicular body
Z_f	the vertical displacements of the front wheel
Z_r	the rear wheel

$\delta(\dots)$	Dirac delta function
δ_{ij}	the Kronecker delta function
ε_{ij}	strain component
ζ	loss factor for a soil exhibiting hysteretic damping
θ_{c}	rotation of vehicular body about the transverse axis
κ	wavenumber
κ_0	datum wavenumber
λ, μ	Lame's constants
λ'	shakedown limit of the pavement system
λ_n	shakedown limit of each layer
λ^w	road wavelength
υ	coefficient of friction between the tire and the ground surface.
$\xi(x)$	Road Roughness
ρ	mass density of the materials
$\sigma_{ij}\ (i,j=x,y,z)$	Stress in Physical Domain
$\sigma_{ij}^{'e}$	a unit elastic response pertaining to the wheel load
$\sigma_{ij}^{'r}$	residual stresses due to accumulated permanent deformation
$\hat{\bar{\sigma}}_{ij}\ (i,j=x,y,z)$	stress in FIT domain
ϕ_k	a stochastic phase angle
φ	material internal friction angle
ω_0	frequency of the harmonic moving load

EXECUTIVE SUMMARY

Pavement design is a process intended to find the most economical combination of layer thickness and material type for the pavement, taking into account the properties of the subgrade soil and the traffic to be carried during the service life of the road. The currently prevalent methods of pavement analysis and design, however, are more or less empirical in U.S., which possess the shortcoming that the important type of pavement distress of rutting related to the accumulation of plastic or permanent deformations cannot be effectively considered. This project proposes an exploratory study on the application of the plasticity theory-based shakedown concept to the analysis and design of pavements under repeated loading, with a more realistic incorporation of the roughness impact of the top pavement layer on the dynamic amplification of vehicle loading as well as on the elastic stress responses in the underlying subsoils.

The main objectives of this research include (a) a vehicle-road coupling model for estimating the additional dynamic vehicle load induced by pavement roughness considering road surface deformation and traveling speed; (b) development of a rigorous analytical solution for the elastic stress fields in asphalt-base-subsoil systems due to the moving surface loads determined above, which is essentially desirable for the subsequent shakedown limit analysis; and (c) proposition of a programming approach to compute the critical shakedown load of the pavement systems in association with an optimized, self-equilibrated residual stress field.

Numerical results from the newly developed vehicle-road coupling model show that the total vehicle load amplification factor ranges from 0.88 to 1.16 under different roughness levels and traveling speeds. This indicates the necessity and importance of incorporating the factors of roughness/vehicle speed in the pavement response analysis. On the other hand, extensive parametric analyses for the shakedown limit show that increases in the pavement cohesion strength and internal friction angle and in the pavement thickness have a positive influence on the calculated shakedown limit value. The analysis results also indicate that there generally exists an optimal Young's modulus ratio between the pavement and subsoil, for which a maximum shakedown load of the pavement system will be reached.

The outcomes of this project on one hand add contributions to the development of a more rational theoretical framework for the pavement design/analysis. On the other hand, the shakedown design approach can prevent the flexible pavement from excessive rutting failure, and hence is of great practical value for prediction/design of the vehicle load, traveling speed, and layer thickness that is required to warrant shakedown state of the pavements (i.e., no excessive rutting) in the long run. It is expected that the dynamic loading evaluation and the plasticity-based shakedown design approach developed in this research could potentially become part of the AASHTO ME for flexible pavement analysis and design.

1. INTRODUCTION

1.1. Vehicle induced dynamic loads

Road surfaces always have different levels of roughness that causes vehicles traveling on pavements to vibrate vertically. As a result, additional dynamic loads are imposed to the pavements. Estimation of road roughness induced additional vehicle loads on the pavement is critically important for pavement analysis and design. In the past decades, active research effort has been exerted to model the road roughness and the induced additional vehicle load *(1-4)*. Power spectral density (PSD) were used by Doddds and Robson *(1)* and Iyengar and Jaiswal *(3)* to describe the road surface roughness. Hardy and Cebon *(2)* simply used half the static load of the vehicle as the road roughness induced additional vehicle load. This approach is easy to apply yet may underestimate/overestimate the additional vehicle load, which is essentially dependent on the road roughness levels, the traveling speed, and the vehicle mechanical properties. Sun and Deng *(4)* studied the statistical characteristics of wheel loads using numerical simulations. The authors found that the induced dynamic loads can be regarded as a Gaussian stationary ergodic process of which the PSD is proportional to the road surface roughness PSD. Recently, to consider the influence of road roughness, a sinusoidal road profile is utilized when estimating the additional vehicle load *(5)*. While this approach appears more advantageous, it is still limited since a real road profile contains multiple wavelength components and is essentially random. To address these limitations, inverse Fourier transformation is used to generate the road roughness $\xi(x)$:

$$\boldsymbol{\xi(x) = \sum_{k=1}^{N} \sqrt{2S(n_k)\Delta n}\cos(2\pi n_k x + \phi_k)} \quad [1]$$

where:

$S(n_k)$ = the power spectrum density function; and

ϕ_k = a stochastic phase angle.

Equation 1 is widely used to estimate the additional vehicle load.

While existing literature in this area advanced the understanding of the characteristics of wheel dynamic loads, there are still several key questions that remain unclear when estimating the loads. First, the vehicle-road interaction which is critically important for pavement on saturated soft subgrade is lacked in most of existing literature. The considerable road surface deformation might increase or decrease the vehicle dynamic loads in different scenarios. Second, the vehicle traveling speed effect is not thoroughly understood in existing research when calculating the vehicle dynamic loads. To address these limitations of existing research, a new vehicle-road coupling model is needed to estimate the additional vehicle load on pavement considering the vehicle-road interaction and the time-variant traveling speed.

1.2. Pavement analysis and design methods

Currently, empirical design and mechanistic-empirical design are two major approaches for flexible pavement design in U.S. The empirical design approach *(7)*, based primarily on the extrapolations from the original American Association of State Highway Officials (AASHO) Road Test conducted from 1958-1960 in Ottawa, Illinois, is not capable of considering the failure mode of the pavement and hence often leads to significant overdesign. The mechanistic-empirical design, more or less resorting to the mechanical models to evaluate the state of stress in a pavement, has

advantage of considering both vehicle loading and material properties so as to select appropriate materials and layer thickness for the pavement. However, the current mechanistic-empirical design only uses the resilient modulus regardless of the plastic properties of the pavement material and ignores the dynamic amplification of the vehicle loading due to the roughness of the pavement. Therefore, pavements designed with these two methods could not effectively prevent the various types of failure governed by the plastic properties of the pavement materials, such as rutting, surface and subsurface slip, and crack formation within its service life.

Plasticity-based shakedown analysis/design *(6)*, in contrast, aims at achieving a long pavement life without deep structural distresses and recently has been advocated as a rational criterion for the "perpetual design" of pavement systems *(8)*. Shakedown is known as a phenomenon that an elastic-plastic structure, though deforms plastically in initial load cycles, responds purely elastically to subsequent load cycles if the applied load is above the yield limit but lower than a critical load. The basic assumption of pavement shakedown design is that the pavement will eventually respond in a resilient manner or will fail with excessive accumulative permanent deformation. The critical vehicle loading, below which shakedown occurs and above which the pavement fails with excessive rutting accumulation, is referred to as the shakedown load/limit. The long-term response of the pavement will be purely elastic if none of its component layers, through their service lives, experiences stress levels exceeding their respective shakedown limits, although the response may well be plastic for a finite number of initial vehicle loading cycles. Shakedown analysis provides an effective solution for perpetual design of pavement systems, and therefore can serve as a potential tool in the design of flexible pavement. The most important task in the use of the shakedown theory in pavement design lies in the determination of the critical shakedown load. If the shakedown limit is determined, it is easy to find a most economical combination of layer thicknesses and material types to prevent failure due to excessive rutting within the service life.

Extensive research works have been conducted to calculate the critical shakedown load either through multilayer elastic theory along with a linear programming *(6, 9-11)* or by taking advantage of the finite element programs procedure *(12-15)*. However, many important factors including the pavement roughness and the dynamic effects induced by vehicle loads, although having significant effects on the pavement responses at high vehicle speed, are generally ignored in these pavement shakedown analyses. Moreover, although shakedown design is more advanced than the existing empirical and mechanistic-empirical design approaches, it has not been yet used in the current flexible pavement design in U.S. It is therefore desirable to develop a rational shakedown design approach, which has the capability to well address all the above-mentioned important issues, so as to contribute better to the perpetual design of pavements in U.S.

1.3. Research objectives and tasks

This research project thus aims to (a) develop a vehicle-road coupling model for estimating the additional dynamic vehicle load induced by pavement roughness considering the traveling speed; (b) derive a rigorous analytical solution for the elastic stress fields in asphalt-base-subsoil systems due to the moving surface loads determined above, which is essentially desirable for the subsequent shakedown limit analysis; and (c) propose a programming approach to compute the critical shakedown load of the pavement systems in association with an optimized, self-equilibrated residual stress field. The major contributions of this research work contain the following four aspects:

(1) A thorough literature review has been conducted on the existing models used for the pavement performance assessment and the estimation of additional vehicle load due to road roughness on the pavement system, with the emphasis on those pertaining to the plasticity-based shakedown analysis of pavement.

(2) Mathematical half and quarter car models have been established and programmed using Matlab. Vehicle-roughness coupling effect is modeled in this proposed method. Road surface deformation is calculated and used to update the initial road roughness profile when determining the vehicle dynamic loading. Given vehicle properties, road roughness profile and traveling speed, the developed Matlab code can be used to calculate vehicle induced dynamic loading acting on the road surface. Extensive parametric studies have been performed to quantify the roughness-vehicle coupling effect. The established vehicle-road coupling model can more accurately (in comparison with the existing methods) estimate the additional dynamic vehicle load induced by pavement roughness considering the traveling speed.

(3) A semi-analytical approach based on the Fourier integral transform technique has been developed to evaluate the stress responses of a multi-layered pavement system that is subjected to static and/or dynamic surface loading, with due account being taken of the additional dynamic vehicle load as already determined in the previous task. The calculated results for the static loading case show an excellent agreement with the existing analytical (Boussinesq) solution, thus indicating the overall correctness and reliability of the proposed integral transform method for the pavement/soil stress analysis. Such obtained stress field, when incorporated into the shakedown analysis framework, essentially enable the pavement shakedown limiting load to be determined.

(4) On leverage of the derived analytical solutions for the elastic stress responses, a framework for the shakedown analysis of pavements under moving traffic loading has been developed based on the objective-oriented program Matlab, by using Melan's low bound shakedown theorem. Extensive parametric analyses have been conducted to investigate the impacts on the pavement shakedown limit of various design factors, such as the Young's modulus ratio, the cohesion ratio between the pavement layers, the vehicle travelling speed, and the dynamic stress amplification coefficient due to the pavement roughness.

2. OBJECTIVES

The main objectives of this research are:

(a) To develop a vehicle-road coupling model for estimating the additional vehicle dynamic load induced by pavement roughness considering the traveling speed;

(b) To derive a rigorous analytical solution for the elastodynamic stress fields in asphalt-base-subsoil systems due to the moving surface loads determined above, which is essentially desirable for the subsequent shakedown limit analysis; and

(c) To propose a linear programming approach to compute the critical shakedown load of the pavement systems in association with an optimized, self-equilibrated residual stress field.

3. LITERATURE REVIEW

3.1. Pavement analysis and design methods

Due to complexities in the behaviors of the constituent materials under traffic loads and environmental conditions, pavement design techniques are still far from advanced in comparison to other branches of geotechnical engineering *(12,16)*. Currently, empirical design and mechanistic-empirical design are two major design approaches for flexible pavement in U.S. The empirical design approach-AASHTO Design Guide, which prevails before 1990 and is still widely used in many states, is primarily based on the observations from the original American Association of State Highway Officials (AASHO) Road Test conducted from 1958-1960 in Ottawa, Illinois. With the empirical design formulas extrapolated from the AASHO Road Tests and some design inputs, required thickness could be determined successively for each layer of a multilayer pavement structure to meet the designed serviceability in whole service life. However, because the empirical design equations are strictly limited to the conditions of the original road tests due to the empirical nature of the method itself, they cannot be easily updated to accommodate new materials, loads types and other conditions. Therefore, pavement designs conducted today using the AASHTO Design Guide, primarily based on the extrapolations beyond the original experimental conditions, often lead to either under design or over design of a multilayer pavement structure. Another major limitation of the AASHTO empirical design is that an empirical rating scale was employed to quantitatively evaluate the serviceability of the pavement, which could not effectively considerer the failure mode, such as the rutting and fatigue cracking, of the pavement.

Mechanistic-empirical pavement design, capable of predicting pavement responses throughout the structure, began to appear in U.S. in the early 1980s, but because of its complexity it became a viable option for pavement design until personal computers were commonly available in the 1990s. In the mechanistic-empirical design, the pavement responses at critical locations are firstly calculated using the multilayer elastic theory, and empirical formulations are then used to correlate the pavement responses to the possible failure modes to check if the pavement thickness and material could meet the designed pavement life. The mechanistic-empirical approach has one distinct advantage over the empirical one in that the mechanistic-empirical approach allows designers to identify all the possible failure models and design accordingly. Moreover, the mechanistic-empirical approach is capable of accommodating to different load levels, new materials as well as other new conditions. Therefore, to yield more reasonable combination of layer thicknesses and material types under designed loads during pavement service life, the pavement design in U.S. is experiencing the transformation from empirical design to mechanistic-empirical design. Although mechanistic-empirical design greatly alleviates many of the shortcomings of the existing empirical design, one major limitation of mechanistic-empirical approach is that the material properties used in design is only the resilient modulus regardless of the strength properties of the material which governs the various type of pavement failure, such as rut formation, surface and subsurface slip and crack formation.

Recognizing that all materials have inherent endurance limits below which no damage will occur, the concept of perpetual pavement design, aims at achieving a long pavement life without deep structural distresses, is proposed recently in U.S. to optimized pavement design. Perpetual pavement design uses the same design procedure with mechanistic-empirical pavement design, the only difference is that the empirical formulations is used to relate the pavement responses to the endurance limits of the pavement materials. Hence, perpetual pavement design is taken as a subset

of mechanistic-empirical design in U.S., which is still very complex in design and cannot get rid of the empirical nature. Another shortcoming of current perpetual pavement design is that plasticity properties of pavement materials are not reasonably considered, thus some failure modes, which are attributed to material plasticity, could not be properly prevented in the design.

3.2. Plasticity-based shakedown concept/theorems

Shakedown is known as a phenomenon that an elastic-plastic structure, though deforms plastically in initial load cycles, responds purely elastically to subsequent load cycles if the applied load is above the yield limit but lower than a critical load. Consider an elastic-plastic (pavement) structure subjected to a cyclic load. Depending on the magnitude of the applied loading, there may exist three distinctive responses/situations of the structure *(17)*. First, if the load level is lower than the elastic limit of the structure, the element behavior anywhere within the structure would be entirely elastic, so that the deformation will fully recover when the cyclic loading is moved away. Second, with the gradual increase of the amplitude of the repeated load, the elastic limit/strength will be surpassed, and some part of the structure will transfer to plastic state from their previous pure elastic response. However, there is a critical load level, below which the plastic deformation will not continuously develop but cease to occur after a certain number of load cycles. In other words, the whole structure responds as if a purely elastic one to the remaining cycles of the loading. If this happens, the structure is considered to have undergone "shakedown" by a process of adaption, and the corresponding critical load/limit (the upper limit under which the structure will eventually go through elastic responses for the future cyclic loads) is termed as a "shakedown limit", or "elastic shakedown limit". Third, if the applied load is further increased/beyond such shakedown limit, the structure will then continue to develop plastic strains for however long the cyclic loading is exerted. This will lead the structure to a final failure state as a result of fatigue or excessive plastic deformation *(17)*. It is obvious that, for structures under variable loads, determination of the critical shakedown limit provides a rational criterion and seems to be very appearing from the design point of view.

The exact determination of shakedown conditions, i.e., the shakedown limit, requires in principle an analysis of the elastic-plastic equilibrium of a structure/body *(18)*. This analysis, however, can only be affected in very simple problems, but not for the practical shakedown problems involving two- or three- dimensional formulations. As noted in Yu *(17)*, in these cases it is hardly possible to derive the exact shakedown limits. Nevertheless, there exist a number of theorems regarding shakedown which essentially eliminate such complicated analysis of the elastic-plastic state, by enabling the upper bound *(19)* and lower bound *(20)* for the shakedown region to be found *(18)*. By employing these lower and upper bound shakedown theorems, one can estimate the shakedown limit of a general elastic-plastic structure in an incomparably simpler manner, requiring only the detailed application of the solution of an approximate elastic problem. The lower bound shakedown theorem was proposed by Melan *(20)*, also known as Melan's shakedown theorem. It states that if any self-equilibrated residual stress field can be found, which, when combined with the elastic stress field produced by the applied loads, does not violate the yield condition anywhere, then shakedown will occur in the structure (20). It provides a lower bound for the shakedown limit and is called the static shakedown theorem since the internal equilibrium equations and the stress boundary conditions can be satisfied. The upper bound shakedown theorem, on the other hand, was proposed by Koiter *(19)*. It can be stated as follows: the structure will not shakedown for given extreme load values, i.e., it will ultimately fail owing to progressive plastic flow, if the energy dissipation introduced by any plastic deformation/rate is smaller than the one induced by the

external load in a single cycle can be found *(19)*. The upper bound shakedown theorem is also called the kinematical theorem because of the plastic strain rate and boundary conditions for velocity involved in the formulation. It should be noted that the application of Koiter's upper theorem involves greater difficulties than the application of Melan's lower theorem *(18)*. They are the two analytical shakedown theorems which assume purely elastic-plastic material, small deformation without considering the inertia and creeping *(21)*. Though these are two different approaches, the shakedown limits obtained from them will converge *(9-10)*. Hence, these two approaches lead lower and upper bounds to the true shakedown limit, respectively *(22)*. Based on these fundamental works, many researchers developed and extended these theorems to consider the material hardening *(23-27)*, the influence of creep *(28, 29)*, temperature-dependent materials *(30)*.

3.3. Shakedown analysis in pavement engineering

Based on the observation from the AASHO Road Tests, the pavement indeed approached a stable state rather than deteriorate continuously after a certain number of relatively small load cycles. In light of this, shakedown theory is extremely suitable to the perpetual pavement design. Indeed, over the past decades, there has been growing interest in the application of the fundamental shakedown theorems to investigate the behavior of flexible pavement system under moving traffic/cyclic loads *(8, 9, 12, 31-36)*. The literature review in this section on the shakedown limit prediction/analysis in pavement engineering is presented in terms of the following three aspects: Laboratory and field tests; numerical analyses; and analytical models.

3.3.1. Laboratory and field tests

To study the shakedown behaviors of granodiorite and sandy gravel materials, a series of cyclic triaxial tests were conducted by Werkmeister *(37-39)*. Their results were obtained by keeping the confining pressure as a constant while changing the vertical stress and were depicted in a chart which is cumulative vertical permanent strain against vertical permanent strain rate. The responses of granular materials can be classified as plastic shakedown when the accumulated plastic strain rate is very small per cycle, plastic creep, and incremental collapse.

Meanwhile, shakedown behaviors of natural soil were also reported through several undrained triaxial laboratory tests. For instance, Sangrey et al. *(40)* controlled the pore water pressure by varying the axial compression with an axial strain rate at around 0.0002% per minute. Their results reported that closed stress-strain and pore pressure-strain hysteresis loops can be measured if the samples achieve a non-failure equilibrium status, on the other hand, the soil samples will reach the effective stress failure status by accumulating the pore pressure. The influence of water content on the shakedown limit was reported by Muhanna et al *(41)* and Yang and Huang *(42)*. It is shown that the high moisture in soil samples, the lower the shakedown limit is.

Considering shakedown phenomena in asphalt pavements have been started from the middle of 1980s. The phenomenon can be observed in full-scale road tests which were done from the AASHO road tests and some road sections in Australia *(32, 43, 44)*. A full-scale pavement, which consists of an asphalt concrete layer, an unbound granular layer and the subgrade soil, an experiment was done by Allou et al. *(45)* in France. Their conclusion reports that rutting gradually tends to stable after around two million repeated loading applied on the pavement, and it demonstrates that the shakedown phenomenon exists in the asphalt pavement structures.

Besides the observations and tests in the field, a number of laboratory tests were also done. For example, Ahmad et al. *(46)* studied the rutting resistance of dense graded hot mixed asphalt using the dynamic modulus Simple Performance test and Wessex wheel tracking device at various temperatures and loading frequencies. Results show that there is a strong correlation between rutting stiffness factor and rutting depth based on the wheel tracking test at 5Hz loading frequency during the temperature in the interval of 40°C and 50°C. Liu et al *(47)* studied the influence of temperature on the shakedown for samples consisting of a dense bituminous macadam layer and a granular layer. Results show that the shakedown limit is highly affected by the temperature. The high temperature will significantly reduce the shakedown limit and accompany a transform of the failure mode from the granular layer failure to the asphalt layer failure.

3.3.2. Numerical analyses

Numerical methods, especially finite element methods, are adopted as a good option to analyze shakedown phenomena in pavement structures. In research conducted under numerical approaches, pavement structures are always discretized into small meshes. As well as optimizations techniques are involved to obtain the shakedown limit. For instance, Raad et al. *(48, 49)* applied the numerical method combined with the Melan's shakedown theorem to a two-layered pavement structure including a top layer over a subgrade layer. Najm *(50)* and Raad et al *(51)* extended this approach to study the shakedown analysis of non-linear stress related to resilient properties in granular materials. The lower bound shakedown theorem was developed in the numerical method with linear approximations by Yu and Hossain *(52)*. The triangular stress-based elements are used, and the optimum residual stress field is determined through these elements before obtaining the shakedown limit based on a linear programming approach. Based on Yu and Hossain *(52)*'s work, Shiau and Yu *(35)* used a displacement bounding method to investigate the pavement deformation at the shakedown status. Though results show a good convergence with Sharp and Brown *(32)*'s solutions, the significant drawback is that if the mesh size is too fine, the size of the linear programming will be excessively large and eventually result in calculation difficulties.

In the numerical method, the full history of the stress-strain curve can be achieved. However, this process is time-consuming and may not be necessary for determining the final shakedown limit which we concern about in the process of pavement design. Compared with it, the shakedown analytical methods (both the Melan's static shakedown theorem and the Koiter's kinematic shakedown theorem) can directly obtain the shakedown limit *(53)*.

3.3.3. Analytical models

Compared with the drawbacks of numerical approaches combined with the linear programming problem, the analytical solution exists the merit in this aspect. To overcome it, Radovsky and Murashina *(34)* proposed the analytical approach for two-dimensional shakedown analysis. Extending their work by assuming a critical plane in which only exists the normal residual stress field, the analytical approach was applied to a three-dimensional homogenous semi-infinite pavement problem under moving Hertz loads by Yu *(9)*. This solution can also be reduced to a two-dimensional case and shows a good convergence with Collins and Cliffe *(33)*'s solutions. And the three-dimensional results provide a good agreement with the ones by Ponter et al. *(54)*'s work which are obtained based on the upper bound shakedown theorem.

A scanning line method was proposed by Krabbenhøft et al. *(36)* to obtain the shakedown limit based on the static bound shakedown theorem of plane strain half-space under moving loads, and

it was developed by Zhao et al. *(53)* to study the influences of various load distributions on the two-dimensional shakedown limit. In this method, both total stresses and residual stresses can be satisfied by the equilibrium equations and yield constraints. Results show that an overvalued shakedown limit may be caused by a relaxed yield constrain of residual stress fields at a high surface friction scenario.

Yu and Wang *(10)* proposed a critical self-equilibrated residual stress field and a simple bisection optimization procedure to solve the three-dimensional shakedown limit. The problem can be reduced to solve a load factor only. A series of studies have been done based on this approach and it was developed to consider more complex cases, such as multi-layered pavement structures, and a multi-layered pavement system with anisotropic materials for each layer *(22, 55-58)*.

The kinematic shakedown theorem also has been widely studied and applied to analyze shakedown problems. The conics method *(32)* was demonstrated by Collins and Cliffe *(33)* that can be explained by the kinematic theorem. They introduced this method to analyze geotechnical problems. Consequently, Collins et al. *(59)* extended this approach to three-dimensional analysis and obtained a good agreement on results with the ones in Ponter et al. *(54)*'s work.

Combining the linear matching method, Ponter and Engelhardt *(60)* firstly analyzed the shakedown phenomenon in metal material. Then it was extended to non-linear geotechnical materials by Boulbibane and Ponter *(16)*. In this method, the non-linear material mechanics behaviors may be determined by solving linear problems with choosing the moduli to vary linearly with time and space *(12)*.

3.4. Research motivation

The above literature review indicates that extensive research works have been conducted to calculate the critical shakedown load either through multilayer elastic theory along with a linear programming *(6, 9-11)* or by taking advantage of the finite element programs procedure *(12-15)*. However, many important factors including the pavement roughness and the dynamic effects induced by vehicle loads, although having significant effects on the pavement responses at high vehicle speed, are generally ignored in these pavement shakedown analyses. In particular, significantly irregular settlement, i.e., pavement roughness, is common phenomenon for a flexible pavement structure constructed on soft subsoils withstanding long-term moving vehicle loads *(61-63)*. The roughness can affect the dynamic stress responses in the pavement *(64)*, which may lead to unrecoverable plastic deformations and collapse failure before the traffic load reaches the designed maximum value. Moreover, although the shakedown design is more advanced than the existing empirical and mechanistic-empirical design approaches, it has not been yet widely used in the current flexible pavement design in the U.S.

It is therefore desirable to develop a rational shakedown design approach, which has the capability to well address all the above-mentioned important issues, to contribute better to the perpetual design of pavements in the U.S. To accomplish this, a vehicle-road coupling model for estimating the additional dynamic vehicle load induced by pavement roughness with constant traveling speed will be first developed. A rigorous, semi-analytical solution for the elastic stress fields in a multi-layered pavement system due to the moving surface loads determined above then will be derived, which is essentially required for the subsequent shakedown limit analysis. Finally, a potential shakedown approach for perpetual flexible pavement design will be proposed by using the Melan's lower bound shakedown theorem, and extensive parametric analyses will be conducted to

investigate the impacts on the pavement shakedown limit of various design factors, such as the Young's modulus ratio, the cohesion ratio between the pavement layers, the vehicle speed, and the dynamic stress amplification coefficient due to the pavement roughness.

4. METHODOLOGY

Dynamic responses of a pavement system under moving vehicular loads are of great importance in the fields of pavement and geotechnical engineering. Exact solution for this problem not only provides the elastic deformations of the pavements that are related indirectly to the permanent plastic strains *(65)*, it also plays an essential role in assessing the lifetime performance of pavements when using a plasticity-based shakedown model to consider rutting *(6,32,66)*. Although great progress has been made on the traffic load-induced dynamic responses of soils/pavements, most of the above-mentioned studies deal with the pavement system simply as a homogeneous elastic/poroelastic half-space. There is still a dearth of research pertinent to the truly multi-layered pavements, and in particular, little information is available regarding the impacts of pavement roughness on the resulting dynamic stresses in individual layers of the pavement systems.

In this presented research, a vehicle-road coupling model is proposed to consider the influence of pavement roughness and its deformation on the traffic load. Numerical dynamic stress fields in a multilayered pavement system are solved based on the Fourier integral transform method (FIT) and the Transmission and Reflection Matrix (TRM) method. The explicit stress expressions can be depicted in the Fourier transform domain, and the stress distributions will be numerically obtained in the MATLAB software package. A computational example will be presented to verify the feasibility of this proposed approach. Consequently, the analytical elastodynamic stress field will be incorporated into the plasticity-based shakedown theory in an attempt to provide an advanced and rational model for analysis and design of a flexible pavement system that could avoid excessive rutting failure within the service life. The shakedown limit can be determined by a bisection method and will be executed in the MATLAB software package.

4.1. Estimation of Vehicle Induced Dynamic Loads on Pavements Using a Vehicle-Road Coupling Model

4.1.1. Vehicle Theoretical Models

Three primary vehicle models have been proposed to study the dynamic loads: quarter-truck model, half-truck model, and full-truck model. Considering that the torsional vibration along the vehicle axis is less significant than vertical vibrations, the half-vehicle model and quarter car model are adopted in this research.

Figures 1 (a) and (b) illustrate a half-vehicle model and a quarter-vehicle model. The equations for the motion of the vehicle are established based on the schematic models. In Figure 1, parameters m_c, I_c, m_f, m_r are half of vehicular body mass, half of vehicular body lateral mass moment of inertia, the mass of a front wheel, and the mass of a rear wheel, respectively; k_{s1}, k_{s2}, c_{s1}, and c_{s2} are the stiffness and damping coefficients of the front and rear suspensions, respectively; k_{t1}, k_{t2}, c_{t1}, and c_{t2} are the stiffness and damping coefficients of the front and rear tires, respectively; s_1 and s_2 are the distance of the center of gravity of the vehicular body from the front and rear axles, respectively. This vehicle model has four degrees of freedom, corresponding to the vertical displacement of vehicular body (Z_c), rotation of vehicular body about the transverse axis (θ_c), the vertical displacements of the front wheel (Z_f) and rear wheel (Z_r).

Kinetic energy of the multi-degree freedom vehicle system can be written as:

$$\boldsymbol{T = T\left(\dot{\xi}_f, \dot{\xi}_r, \dot{z}_c, \dot{\theta}_c, \dot{z}_r, \dot{z}_f; m_f, m_r, s_1, s_2\right)} \quad [2a]$$

Potential energy of the multi-degree freedom vehicle system can be written as:

$$\boldsymbol{V = V(\xi_f, \xi_r, z_c, \theta_c, z_r, z_f; m_c, I_c, m_f, m_r, s_1, s_2)} \quad [2b]$$

Substituting Equations 10a and 10b into the Euler-Lagrangian equation yields the equation of motion of the half-vehicle model expressed in a matrix form as follows:

$$\boldsymbol{M_v\ddot{Z} + C_v\dot{Z} + K_vZ = F_v} \quad [3]$$

where:

$\dot{Z}$ and $\ddot{Z}$ = the first and second derivatives of Z with respect to time t, respectively;

M_v, C_v, and K_v = the system mass, damping and stiffness matrices; and

F_v = the force vector.

$$\boldsymbol{Z = [Z_c, \theta_c, Z_f, Z_r]^T, \quad M_v = [m_{ij}]_{4\times4}} \quad [4a]$$

where:

m_{ij} = the element of the mass matrix.

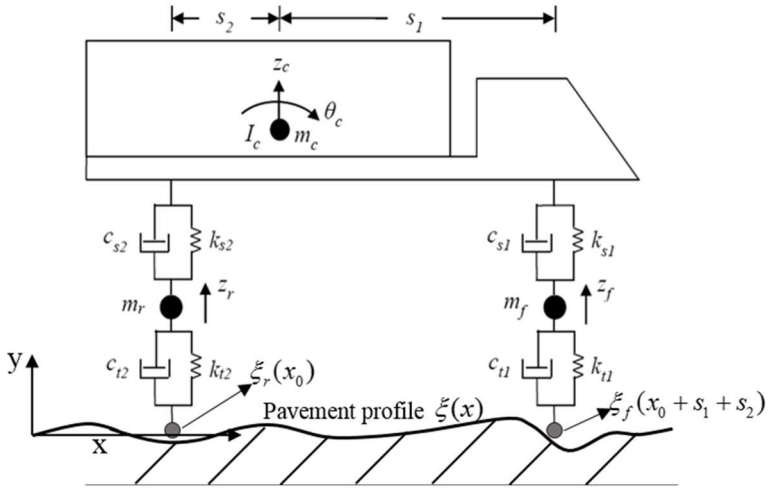

(a)

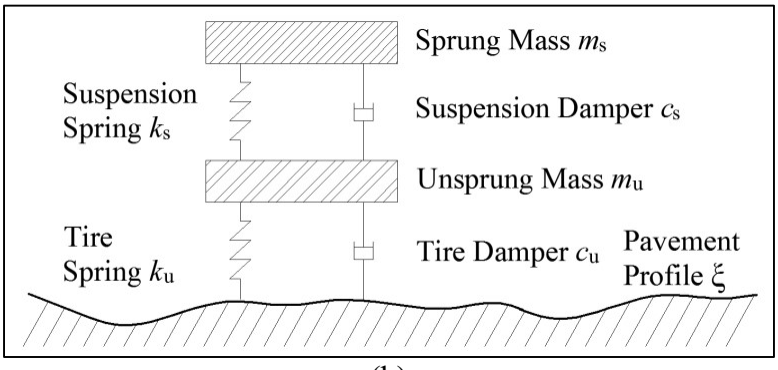

(b)

Figure 1. Half-vehicle vibration model: (a) Half-vehicle model and (b) Quarter-vehicle model.

Specific mathematical expression of the mass matrix elements will be determined during the project. The stiffness and damping matrices are:

$$\boldsymbol{K_v} = \left[\boldsymbol{k_{ij}}\right]_{\boldsymbol{4\times4}}, \quad \boldsymbol{C_v} = \left[\boldsymbol{c_{ij}}\right]_{\boldsymbol{4\times4}} \tag{4b}$$

where:

k_{ij} and c_{ij} = the elements of the stiffness and damping matrices to be determined during the project. The generalized force vector can be expressed as:

$$F = [f_1\left(m_c, \ddot{\xi}_f, \ddot{\xi}_r, s_1, s_2\right), f_2\left(I_c, \ddot{\xi}_f, \ddot{\xi}_r, s_1, s_2\right),$$
$$f_3\left(m_f, \ddot{\xi}_f\right), f_4\left(m_r, \ddot{\xi}_r\right)] \tag{5}$$

where:

f_1, f_2, f_3, and f = the generalized force vector components corresponding to the four degrees of freedom.

The explicit formulas will be derived during the project.

It is worth to note that closed-form steady-state solution of Equation 3 can be derived if the road roughness is represented by a harmonic function, e.g.,

$$\boldsymbol{\xi(x) = A_0 e^{i2\pi vt/\lambda^w} = A_0 e^{i\omega t}} \tag{6}$$

where:

λ^w= the road wavelength; and

v = the traveling speed.

In the proposed research, a more general road roughness profile generated using measured data (see support letter) and the road roughness PSD, Equation 1 will be adopted. In this case, the transient solution of Equation 3 will be solved numerically. In this research, Equation 3 are solved numerically using Newmark-method method. MATLAB codes were developed to implement the Newmark-method to solve for the transient dynamic responses of the vehicle and the wheel dynamic loads on pavement.

4.1.2. Additional Vehicle Load Calculation via Iterations

Vehicle load transmitted from the wheel to the pavement can be expressed as:

$$\boldsymbol{Q = Q_{sta} + Q_{dyn}} \tag{7}$$

where:

Q_{sta} = the static load due to self-weight; and

Q_{dyn} = the additional vehicle load induced by road roughness.

On the basis of the calculated vehicle response, the static and dynamic load of the rear and front wheels can be expressed as:

$$\boldsymbol{Q_{sta} = m_c g \frac{s_1}{s_1+s_2} + m_r g} \quad [8a]$$

$$\boldsymbol{Q_{dyn} = -(\dot{Z}_r - \dot{\xi}_r)c_{t2} - (Z_r - \xi_r)k_{t2}} \quad [8b]$$

$$\boldsymbol{Q_{sta} = m_c g \frac{s_2}{s_1+s_2} + m_f g} \quad [8c]$$

$$\boldsymbol{Q_{dyn} = -(\dot{Z}_r - \dot{\xi}_f)c_{t1} - (Z_f - \xi_f)k_{t1}} \quad [8d]$$

Equations 8a - 8b and Equations 8c - 8d are for real and front wheel, respectively.

4.1.3. Vehicle-Road Coupling Model

It is worthy to note that the road surface deformation caused by vehicle load is not considered in Equation 8. For relatively soft road pavement and foundation, the large vehicle load will cause significant deformation which will further amplify the additional vehicle load. To model this complex procedure, a vehicle-road coupling model will be developed in this research task.

Figure 2 illustrates the flowchart to calculate the total vehicle load Q in an iterative manner which is described as follows:

1) In the beginning, generate the road roughness $\xi_0(x)$;

2) At a given time instant t, determine the initial vehicle load $Q_1(t)$ using Equations 7 and 8;

3) Calculate the deformation $\delta_1(t)$ caused by $Q_1(t)$, update road profile $\xi_1(t) = \xi_0(t) + \delta_1(t)$;

4) Update F^{i+1} which is a function is of $\ddot{\xi}(x)$, Equation 5, and determine $Q_1(t)$;

5) If $|[Q_2(t) - Q_1(t)]/Q_1(t)| \leq \varepsilon$, end iteration and output Q; else repeat steps 3) and 4).

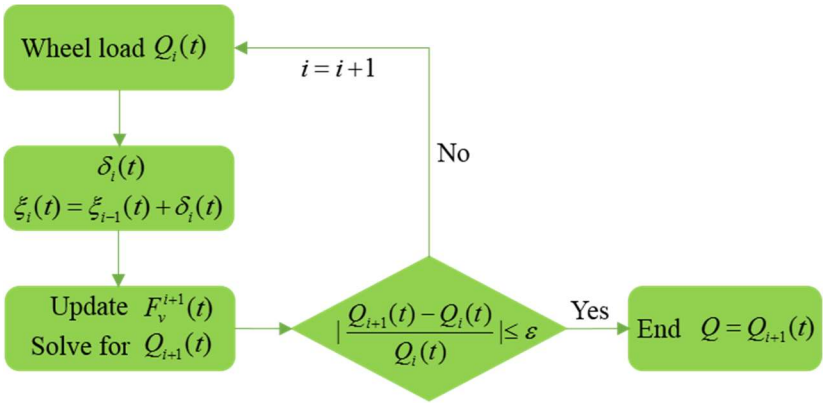

Figure 2. Flowchart of the vehicle-road coupling model.

Through applying the proposed flowchart described above, the time series of the total vehicle load including the static load and the additional dynamic load can be calculated for a given road profile with the preselected vehicle mechanical properties and predefined time-variant traveling speed.

4.1.4. Road surface deformation

A key step of the road-vehicle coupling model is to determine the vehicle dynamic load-induced road surface deformation. In this project, the proposed formula by FIT method is adopted to

calculate road surface deformation. Figure 3 shows a semi-infinite space subsoil loaded by a moving vehicle with a traveling speed of v.

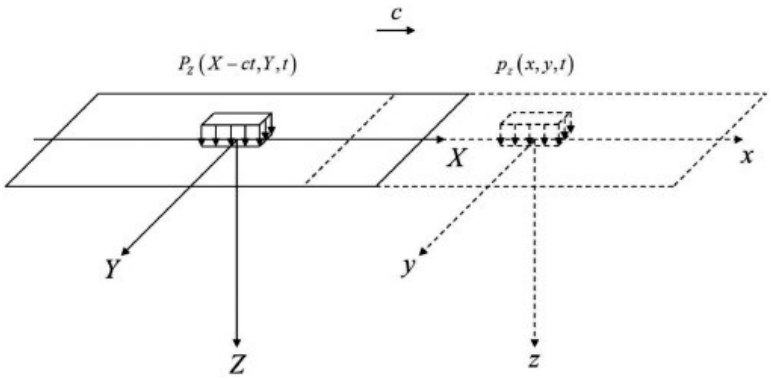

Figure 3. Schematic of vehicle-pavement interaction.

The transient vertical displacement at the road surface can be determined via numerical inverse FIT of Equation 13a when z is 0. MATLAB codes have been developed to calculate the road surface deformation under given roughness level and traveling speed v.

4.1.5. Vehicle Properties

The front and rear axles of the single unit truck in *(3)* are used for simulations in this study. Table 1 lists the mechanical properties of the quarter-truck model of this truck. These two sets of parameters are assigned to a quarter-car model as shown in Figure 1 respectively, which yields the two vehicle models used for simulations in this study.

Table 1. Parameters of quarter-truck model.

parameter	description	front axle	rear axle
m_s	sprung mass	2,500	4,450
m_u	unsprung mass	270	550
c_s	suspension damping constant	15,000	15,000
c_u	tire damping constant	2,000	2,000
k_s	suspension spring constant	200,000	1,150,000
k_u	tire spring constant	800,000	1,800,000

4.1.6. Roughness Generation

The inverse fast Fourier transform (IFFT) of the power spectral density (PSD) of a road profile (ξ provides a suitable model to represent profiles of different roughness levels *(67, 68)*. For this analysis, the second-order forward difference provides a numerical approximation of the second derivative of the profile ($\ddot{\xi}$) *(69)*.

In terms of the International Organization for Standardization (ISO) *(70)*, the PSD of the elevation profile $S_\xi(\kappa)$ can be expressed as:

$$S_\xi(\kappa) = \begin{cases} S_\xi(\kappa_0)\left(\frac{\kappa}{\kappa_0}\right)^{-n_1} & \frac{\kappa}{\kappa_0} \le 1 \\ S_\xi(\kappa_0)\left(\frac{\kappa}{\kappa_0}\right)^{-n_2} & \frac{\kappa}{\kappa_0} > 1 \end{cases} \quad [9]$$

where:

κ = the wavenumber (cycle/m);

κ_0 = the datum wavenumber (cycle/m); and

$S_\xi(\kappa_0)$ = the PSD at κ_0 or initial PSD (m^3/cycle).

For typical profiles, Cebon *(71)* recommended $n_1 = 3$, $n_2 = 2.25$, and $\kappa_0 = 1/2\pi$ cycles/m. Table 2 summarizes the qualitative relationship between the roughness classification and the initial PSD. That is, higher values of $S_\xi(\kappa_0)$ correspond to rougher roads. Sayers and Karamihas *(72)* indicate that the IRI quarter car model does not respond to spatial wavelengths that fall outside 1.3 m to 30 m. Therefore, a range of κ from 0.02 cycle/m to 5 cycle/m will conservatively excite the IRI quarter car model. Figure 4 shows the road profile generated at $S_\xi(\kappa_0) = 3.2 \times 10^{-5}$ m^3/cycle. The generated road profiles will be used for the vehicle-pavement interaction analysis in this study.

Table 2. Relationship between Roughness Classification and Initial PSD.

Roughness classification	$S_\xi(\kappa_0)$, 10^{-6} m^3/cycle
Very good	2-8
Good	8-32
Average	32-128
Poor	128-512
Very poor	512-2048

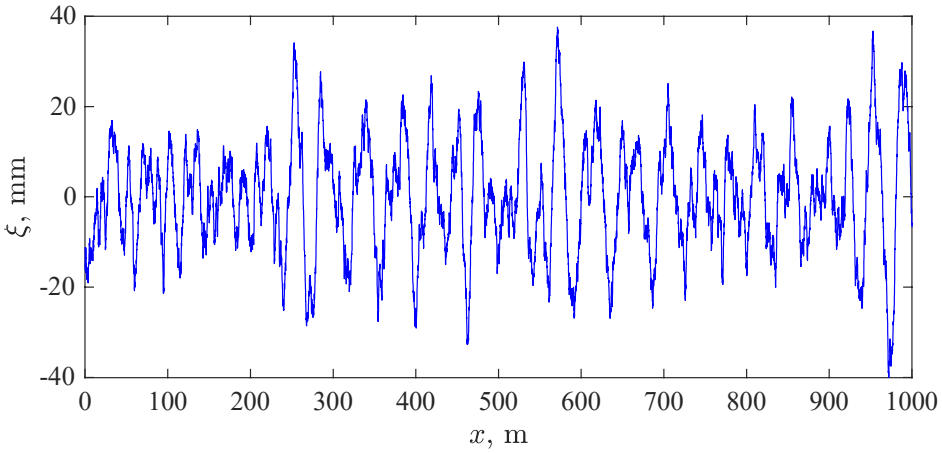

Figure 4. Generated road profile by IFFT method at $S_\xi(\kappa_0) = 3.2 \times 10^{-5}$ m^3/cycle.

4.2. Dynamic Responses in a Multilayered Pavement System

4.2.1. Estimation of Dynamic Responses Using a Semi-Analytical Method

Considering a vertical uniform rectangular load q and a horizontal one p with size $2a * 2b$ moves on the surface of an elastic multi-layer pavement system, as shown in Figure 5. The load moves along with the positive direction of the x-axis with a constant velocity v.

The elastodynamic governing equation can be expressed as follows in an elastic layer *(73)*,

$$\mu u_{i,jj} + (\lambda + \mu) u_{j,ji} = \rho \ddot{u}_i \quad [10a]$$

$$\lambda = (1 + i\zeta)\lambda^* \quad [10b]$$

$$\mu = (1 + i\zeta)\mu^* \quad [10c]$$

where:

u_i ($i = x$, y, and z) = the displacements of the pavement/subsoil; the dot over a variable denotes the differentiation with respect to time t; the subscript comma (,) denotes a partial derivative with respect to the Cartesian coordinates;

ρ = the mass density of the materials;

λ, μ = Lame's constants;

ζ = a loss factor for a soil exhibiting hysteretic damping;

i = the unit imaginary; and

λ^*, μ^* = the regular constants, respectively.

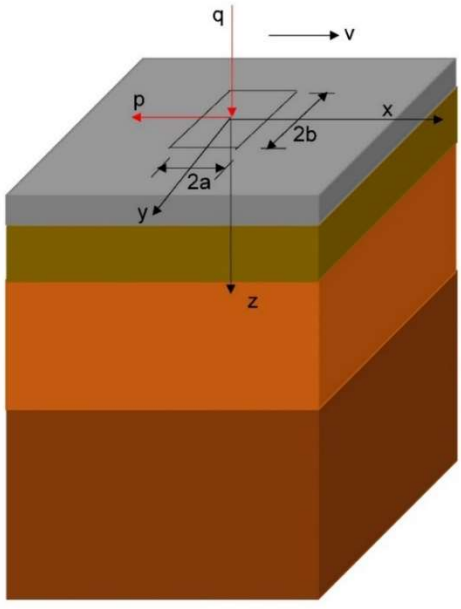

Figure 5. Profile of a multilayered pavement system.

The constitutive relations of the pure elastic medium can be represented as the following form,

$$\sigma_{ij} = \lambda\delta_{ij}\theta + 2\mu\varepsilon_{ij} \quad [11]$$

$$\theta = u_{i,j} \quad [12]$$

where:

σ_{ij} = the stress component;

ε_{ij} = the strain component;

δ_{ij} = the Kronecker delta function.

Fourier integral transform method (FIT) is applied to solve Equations 10 and 11. In this way, displacement components can be solved and expressed as follows,

$$\bar{\bar{u}}_z = \chi_1(Ae^{r_1 z} - Be^{-r_1 z}) + Ce^{r_2 z} + De^{-r_2 z} \quad [13a]$$

$$\bar{\bar{u}}_y = i\frac{\chi_1}{r_1}\eta(Ae^{r_1 z} + Be^{-r_1 z}) + Ee^{r_2 z} + Fe^{-r_2 z} \quad [13b]$$

$$i\xi\bar{\bar{u}}_x = \chi_2(Ae^{r_1 z} + Be^{-r_1 z}) - r_2(Ce^{r_2 z} - De^{-r_2 z}) - i\eta(Ee^{r_2 z} + Fe^{-r_2 z}) \quad [13c]$$

$$r_1 = \sqrt{\xi^2 - \eta^2 - \vartheta^2} \quad [13d]$$

$$r_2 = \sqrt{\xi^2 - \eta^2 - l^2} \quad [13e]$$

$$\vartheta^2 = \frac{\rho^{\ 2}}{\lambda+2\mu} \quad [13f]$$

$$l^2 = \frac{\rho^{\ 2}}{\mu} \quad [13g]$$

$$\chi_1 = -\frac{S^2}{l^2-\vartheta^2} \quad [13h]$$

$$S^2 = \frac{r_1(\lambda+\mu)}{\mu} \quad [13i]$$

$$\chi_2 = (1 + \chi_1\frac{\eta^2}{r_1} - \chi_1 r_1) \quad [13j]$$

where:

A, B, C, D, E and F = constants coefficients.

Submitting Equation 13 into Equation 11, stress fields can be expressed as follows,

$$\bar{\bar{\sigma}}_{zz} = (\lambda + 2\mu\chi\gamma_1(Ae^{\ 1z} + Be^{-\ 1z}) + 2\mu\gamma_2(Ce^{\ 2z} - De^{-\ 2z}) \quad [14a]$$

$$\bar{\bar{\sigma}}_{yz} = \mu[2i\eta\chi(Ae^{\ 1z} - Be^{-\ 1z}) + i\eta(Ce^{\ 2z} + De^{-\ 2z}) + \gamma_2(Ee^{\ 2z} - Fe^{-\ 2z})] \quad [14b]$$

$$i\xi\hat{\hat{\sigma}}_{xz} = (a_1\gamma_1 - \chi\xi^2)Ae^{\ {}_1z} - (a_2\gamma_1 - \chi\xi^2)Be^{-\ {}_1z}$$
$$-(\gamma_2^2 + \xi^2)(Ce^{\ {}_2z} + De^{-\ {}_2z}) - i\eta\gamma_2(Ee^{\ {}_2z} - Fe^{-\ {}_2z}) \quad [14c]$$

For a multi-layered pavement system analysis, some essential assumptions are made regarding boundary and continuity conditions. Properties of material in each layer are assumed to be homogenous, isotropic, and elastic. The non-bottom layers are assumed to be infinite in horizontal directions but of finite depth, while the bottom layer is infinite in both directions.

Coefficients in Equations 13 and 14 can be solved combined with boundary conditions and continuous functions between each layer. The continuity conditions are reflected in the interface between each layer, which means that the stress and displacement components on the interface should be equivalent.

Because of the continuous conditions, there are six continuous equations on each interface which are listed as follows,

$$\hat{\hat{u}}_x^{(j)}(\xi,\eta,z_j) = \hat{\hat{u}}_x^{(j+1)}(\xi,\eta,z_j) \quad [15a]$$
$$\hat{\hat{u}}_y^{(j)}(\xi,\eta,z_j) = \hat{\hat{u}}_y^{(j+1)}(\xi,\eta,z_j) \quad [15b]$$
$$\hat{\hat{u}}_z^{(j)}(\xi,\eta,z_j) = \hat{\hat{u}}_z^{(j+1)}(\xi,\eta,z_j) \quad [15c]$$
$$\hat{\hat{\sigma}}_{zx}^{(j)}(\xi,\eta,z_j) = \hat{\hat{\sigma}}_{zx}^{(j+1)}(\xi,\eta,z_j) \quad [15d]$$
$$\hat{\hat{\sigma}}_{zy}^{(j)}(\xi,\eta,z_j) = \hat{\hat{\sigma}}_{zy}^{(j+1)}(\xi,\eta,z_j) \quad [15e]$$
$$\hat{\hat{\sigma}}_{zz}^{(j)}(\xi,\eta,z_j) = \hat{\hat{\sigma}}_{zz}^{(j+1)}(\xi,\eta,z_j) \quad [15f]$$

the upper script represents the $j-th$ layer as referring to Figure 6.

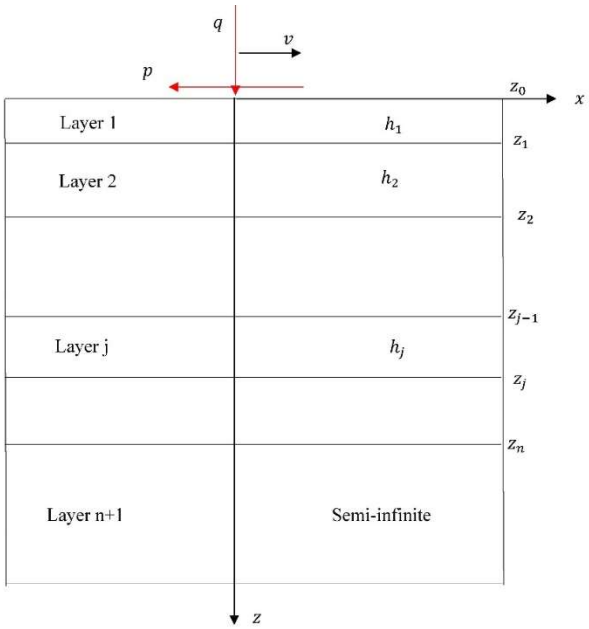

Figure 6. Profile of the section x-z for a multilayered pavement system.

The boundary conditions are that the ground surface is free of shearing and normal stresses outside the loaded area. Thus, the stress σ_{zy} is zero at the ground surface (z=0) since the friction force does not exist on the y-axis which is vertical to the moving direction. In the practical case, the contact area between a tire and the ground surface should be an ellipse *(74)*. But it is replaced by the rectangle area because of the geometrical complexity of the ellipse in the mathematics analysis *(75)*. In this way, the moving surface rectangle load in alignment with the two horizontal coordinates is shown as

$$\sigma_{zz}(x,y,0) = -qe^{i\ {}_0t}[H(x-vt+a)-H(x-vt-a)]*$$
$$[H(y+b)-H(y-b)] \quad [16a]$$

$$\sigma_{zx}(x,y,0) = \upsilon * \sigma_{zz}(x,y,0) \quad [16b]$$

$$\sigma_{zy}(x,y,0) = 0 \quad [16c]$$

where:

q = the constant magnitude of the moving load;

ω_0 = the frequency of the harmonic moving load;

t = time;

$H(\dots)$ = the Heaviside function;

v = the velocity of the moving load;

a, b = the half length of each side of the rectangular contact area; and

υ = the coefficient of friction between the tire and the ground surface.

The stress boundary conditions can be expressed as the following form under the FIT,

$$\hat{\bar{\sigma}}_{zz}(\xi,\eta,0) = -8\pi q \frac{sin(\xi a)\, sin(\eta b)}{\xi\eta}\delta(\omega-\omega_0+\xi v) \quad [17a]$$

$$\hat{\bar{\sigma}}_{zx}(\xi,\eta,0) = \upsilon * \hat{\bar{\sigma}}_{zz}(\xi,\eta,0) \quad [17b]$$

$$\hat{\bar{\sigma}}_{zy}(\xi,\eta,0) = 0 \quad [17c]$$

where:

$\delta(\dots)$ = the Dirac delta function.

The propagator matrix method was applied to solve the coefficients for a layered half-space under dynamic loads *(76, 77)*. The finite element method was developed to solve the dynamic responses in water-saturated layered half-space *(78)*. However, for large layer thickness and high-frequency cases, it is difficult to achieve results by the typical propagator matrix method because the mismatched exponential terms exist between layers *(79, 80)*. To solve this problem, Luco and Apsel *(81, 82)* proposed the transmission and reflection matrix (TRM) method which can eliminate the mismatched exponential terms and obtain the coefficients for each layer in the wavenumber domain.

Based on the TRM method and combining Equations 15 and 17, the coefficients of each layer can be solved, and furthermore, all the stresses and displacements in the Fourier domain are readily known.

4.2.2. Numerical Inversion of Fourier Integral Transforms

Though the stress and displacement fields in the wavenumber domain are obtained, it is necessary to transfer them into the Cartesian-coordinate domain, and then use them in the following pavement system shakedown analysis. However, it is difficult to show explicit expressions of inverse FIT. Jones et al. *(75)* proposed that the ξ- and η-axis of integrals in the wavenumber domain must be truncated at a large value which is to avoid aliasing and leaking during the process of the inverse FIT. In this paper, $-16 \leq \xi, \eta \leq 16$ are applied on integral limits, and a MATLAB code is used to conduct the inverse FIT. For the low moving speed dynamic loading, it can be considered as the static case at the initial condition (t=0). Figure 7 shows the comparison of vertical normal stresses, σ_{zz}, between the results by the currently proposed method and those from the Boussinesq solution. The parameters used in the calculation are the same in each layer, in which a multi-layer pavement system reduces to a semi-infinite subsoil. The values of each parameter are listed in Table 3.

Table 3. Parameters of the moving load and pure elastic soil.

Parameter	Value	Parameter	Value
q (Pa)	50000	μ^* (N/m^2)	$2 * 10^7$
a(m)	0.5	λ^* (N/m^2)	$2 * 10^7$
b(m)	0.5	ζ	0.03
v (m/s)	1	ρ (kg/m^3)	$2 * 10^3$
ω_0	0	t (s)	0
υ	0		

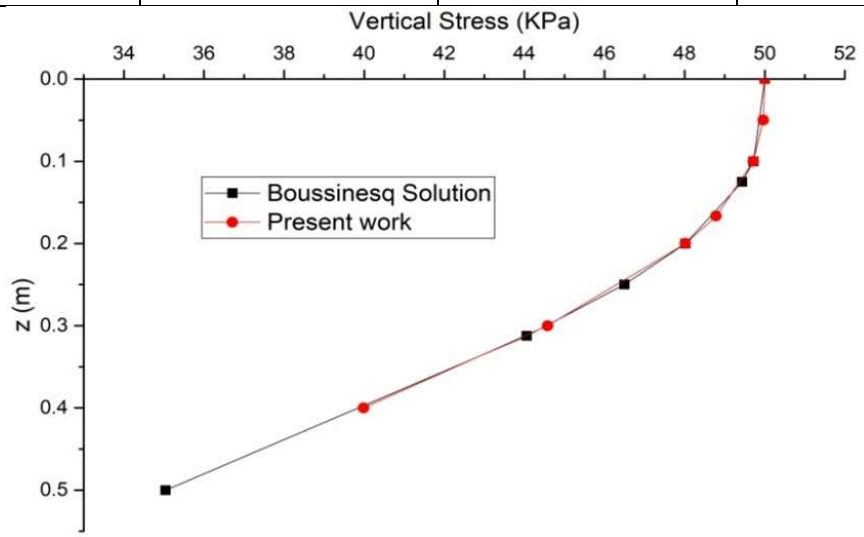

Figure 7. Comparison vertical stresses between the FIT method and Boussinesq solution.

4.3. Lower Bound Shakedown Theorem

According to the shakedown theorem *(6)*, if any equilibrium residual stress distribution can be found, which together with elastic stress fields produced by the repeated traffic loading does not exceed the yield condition at any time, then the desirable shakedown will occur and the permanent plastic strains in the pavement layers, although may be accumulated to a certain level, will be bounded. Mathematically, the above statement leads to the following expression,

$$f(\lambda\sigma_{ij}^{\prime e} + \sigma_{ij}^{\prime r}) \leq 0 \quad [18]$$

where:

f = the yield criterion of pavement system materials, e.g., the commonly used Mohr-Coulomb failure criterion;

$\sigma_{ij}^{\prime e}$ = a unit elastic response pertaining to the wheel load of $Q_{unit} = Q_{sta,unit} + Q_{dyn,unit}$;

$\sigma_{ij}^{\prime r}$ = the residual stresses due to accumulated permanent deformation; and

λ = a load factor giving $Q = \lambda Q_{unit}$.

Yu and Wang *(10)* proposed a bisection method for calculating the low-boundary shakedown limits under static loads. In their work, only the normal residual stress on the moving load direction is considered, the other residual stresses will be eliminated because they are anti-symmetric stresses under the normal stress in a semi-half homogenous space *(9)*. Thus, stresses which are used for shakedown analysis can be expressed as,

$$\sigma_{xx} = \lambda\sigma_{xx}^{e} + \sigma_{xx}^{r} \quad [19a]$$

$$\sigma_{zz} = \lambda\sigma_{zz}^{e} \quad [19b]$$

$$\sigma_{xz} = \lambda\sigma_{xz}^{e} \quad [19c]$$

where:

σ^e = the elastic stress component; and

σ^r = the residual stress component.

Substituting Equation 19 into Equation 18, the Melan's lower bound shakedown can be expressed as follows by assuming the mechanical behavior of materials of the pavement system satisfying the Mohr-Coulomb yield criterion

$$f = (\sigma_{xx}^{\prime r} + M)^2 + N \leq 0 \quad [20a]$$

$$M = \lambda(\sigma_{xx}^{\prime e} - \sigma_{zz}^{\prime e}) + 2\tan\phi(c - \lambda\sigma_{zz}^{\prime e}\tan\varphi) \quad [20b]$$

$$N = 4(1 + \tan^2\phi)[(\lambda\sigma_{xz}^{\prime e})^2 - (c - \sigma_{zz}^{\prime e}\tan\varphi)^2] \quad [20c]$$

where:

c = material cohesion; and

φ = the material internal friction angle.

Equation 20a shows a relationship between λ and f. Here, the residual normal stress σ_{xx}^{r} is the only unknown parameter in Equation 20a. In this way, the low-boundary shakedown limit λ_n (n represents the $n\text{-}th$ layer) of each layer can be determined through determining σ_{xx}^{r} to satisfy Equation 19 by a bisection method programming in MATLAB software. Introducing λ' represents the shakedown limit factor for a multi-layered pavement system, and the relationship between λ' and λ_n is shown as follows,

$$\lambda' = \min\{\lambda_n\} \quad [21]$$

4.4. Computational Model for Obtaining Shakedown Limits

Referring to Figure 8, a simplified two-layer pavement is applied to explore influences of various material properties of pavement and subsoil. A vehicle is moving at a speed of v on the pavement surface along with the positive of the x-axis. The top layer (i.e. Layer 1) represents the pavement layer, and the bottom layer (i.e. Layer 2) constitutes a half-space subsoil. Material properties are shown in Table 4. The length of the contact area $2a * 2b$ equals 0.2*0.3 m.

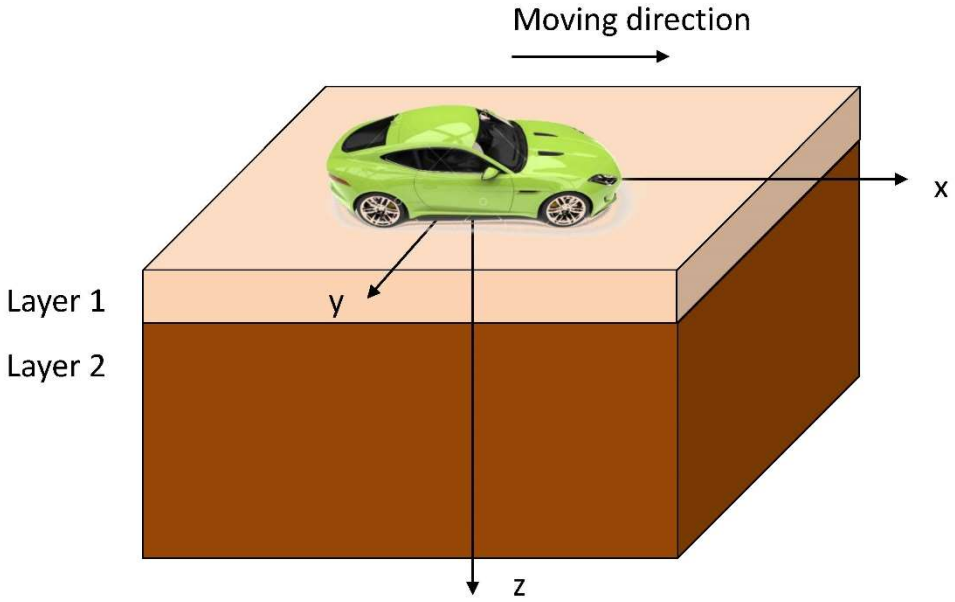

Figure 8. Computational model for a two-layer pavement system.

Table 4. Material parameters used in the two-layer pavement system.

Layer	Young's modulus E (MPa)	Poisson's Ratio ν	Density ρ (kg/m^3)	Cohesion c (kPa)	Internal friction angle φ (°)
1(Pavement)	50 - 5000	0.25	2000	10-100	0 - 45
2(Subsoil)	50	0.25	2000	10	0 - 45

It is well known that a larger numerically computational region can provide a more accurate result. However, computation efficiency is another important factor that cannot be ignored in numerical

computations. Especially for practical engineering, it is not feasible to spend a long time on obtaining results of a single scenario. To consider the efficiency problem, the computational region on the x-, y-, and z-direction is $16a$, $2b$, $4h_1$, respectively, where h_1 is the thickness of the first layer. Two bases force us to choose it as shown above. One is that the traffic load-induced stress decreases to about 5% of the amplitude of the moving load, which satisfies the requirement in civil engineering. For example, if Young's modulus ration, E_1/E_2, is 10 between the two layers, the vertical additional stress σ_{zz} at the point of ($5a$, 0, $0.5h_1$) is 34.8 Pa under a 50 kPa uniform distributed moving load with 20 m/s which is applied on the origin of the coordinate system. It is easy to find that the stress value is 0.07% of the moving load so that its effect can be ignored in engineering design. On the other hand, the shakedown limit will not change if the computational domain expands over $16a$*$2b$*$4h_1$. It shows that a larger computational domain can provide more results in stress fields, but the extra stress fields may not be helpful in changing the shakedown limit. Therefore, choosing the region as $16a$*$2b$*$4h_1$ is reasonable and efficient.

5. ANALYSIS AND FINDINGS

5.1. Results and Discussions of a Vehicle-Road Couple Model

This section presents the results of the road surface deformation and vehicle dynamic loads. The solution scheme is illustrated in Figure 2. At each time step, the pavement's deformation is solved using the FIT. The calculated deformation is then used to update the road profile which is in turn fed back into the program to update the wheel dynamic loads and the pavement's deformation. This process is iterated until the preset convergence criterion is reached. The resultant vehicle response and pavement's deformation are recorded and the analysis proceeds to the next time step. In this study, the influence of road roughness level and vehicle speed on the resultant wheel dynamic loads is investigated. Detailed results and discussions are as follows.

First, a case study on the quarter-car model listed in Table 1 is implemented using a typical roughness level and vehicle traveling speed. Next, the influence of roughness level and vehicle speed will be investigated using the quarter-car model and the property values of rear axle in Table 1.

5.1.1. Case 1: $S_\xi(\kappa_0)$ = 3.2×10-5 m^3/cycle and v = 22.22 m/s

The roughness level with $S_\xi(\kappa_0) = 3.2 \times 10^{-5}$ m^3/cycle is used in this analysis, and it is the boundary of good and average roughness categories as shown in Table 2. The vehicle speed v = 22.22 m/s is used because it is the speed used to calculate the international roughness index (IRI). In this subsection, the road surface deformation and wheel dynamic loads at front and rear axles are determined and presented as follows.

Front axle: Figures 9 through 11 compare the results of vehicle-pavement interaction analysis before and after considering the influence of pavement deformation under the vehicle loads. As shown in the Figure 9, the pavement deformation leads to instant variation of roughness profile and thus can change the dynamic behavior of vehicle and the interaction forces. Figure 9(b) is a zoomed plot of data in Figure 9(a) from 0 to 20 m. It can be observed in Figures 9 (a) and (b) that due to the vehicle dynamic loads and the downward pavement deformation, the road profile is shifted downward by a certain amount, which is approximately consistent along the entire length of the road section. In comparison, Figure 9 (b) illustrates that the road roughness profile has been slightly changed, which will not cause significant variation to the vehicle vertical dynamic responses. As a result, small differences in vehicle responses and dynamic interaction forces can be observed in Figure 10 and 11. The maximum change of dynamic interaction force is around 4.0%.

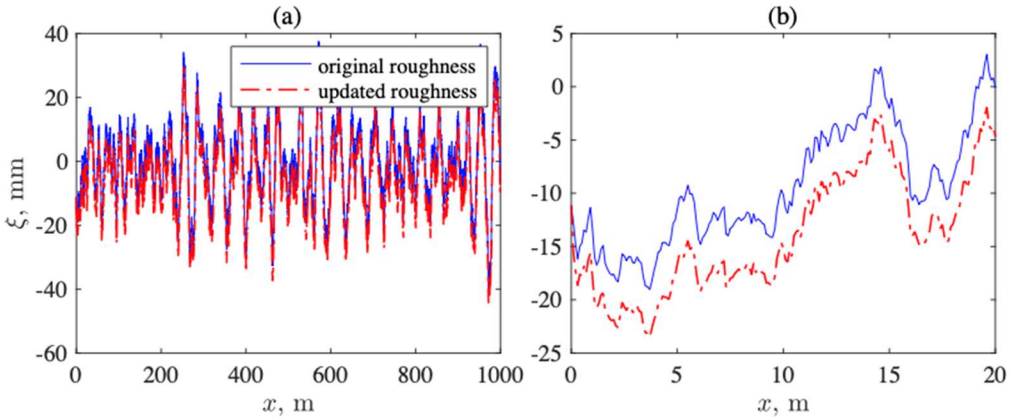

Figure 9. Comparison of roughness profile before and after update. (a) results of the full 1000 m road section; (b) results of the road section of the first 20 m.

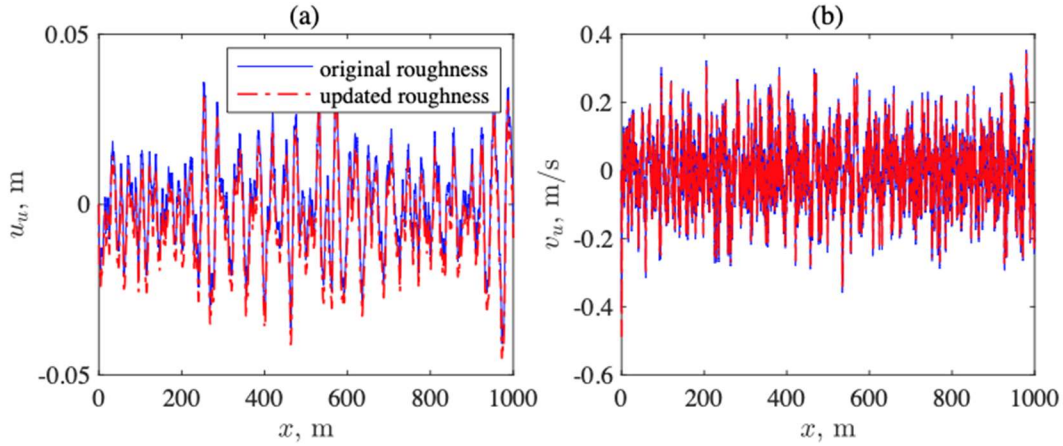

Figure 10. Comparison of vehicle responses before and after update. (a) displacement of the upsprung mass; (b) velocity of the unsprung mass.

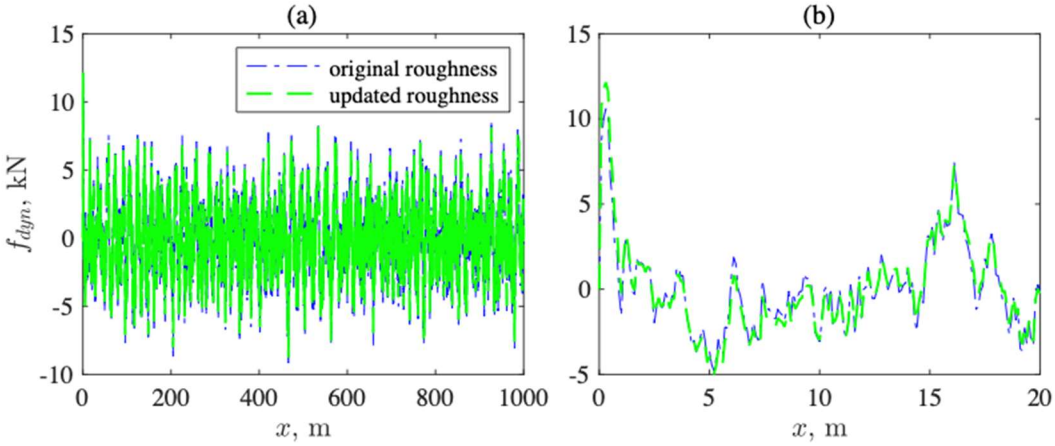

Figure 11. Comparison of dynamic interaction force before and after update. (a) results of the full 1000 m road section; (b) results of the road section of the first 20 m.

Rear axle: When the rear axle is used for analysis, the variations caused by the pavement deformation become more considerable because of the increased weight of the corresponding

quarter-car model, which can be observed from the comparisons presented in Figures 12 to 14. Figure 12 shows that in addition to the downward shift due to the vehicle load, the road profile is significantly smoothened. This phenomenon is not obviously observed in the case with the front axle (Figure 9). As a result of this smoothening effect, the resulting dynamic interaction force is affected to a more extent than the previous case, as shown in Figure 14, and the maximum change is reduced to around 2.3%.

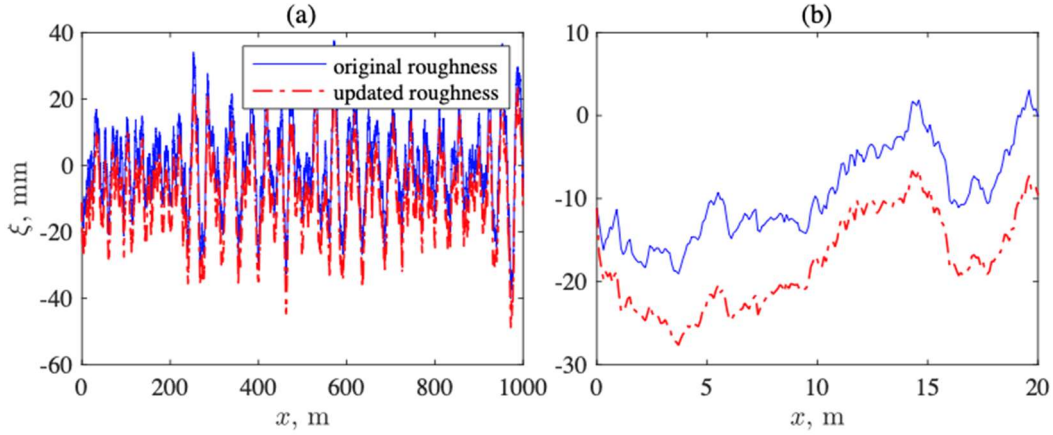

Figure 12. Comparison of roughness profile before and after update. (a) results of the full 1000 m road section; (b) results of the road section of the first 20 m.

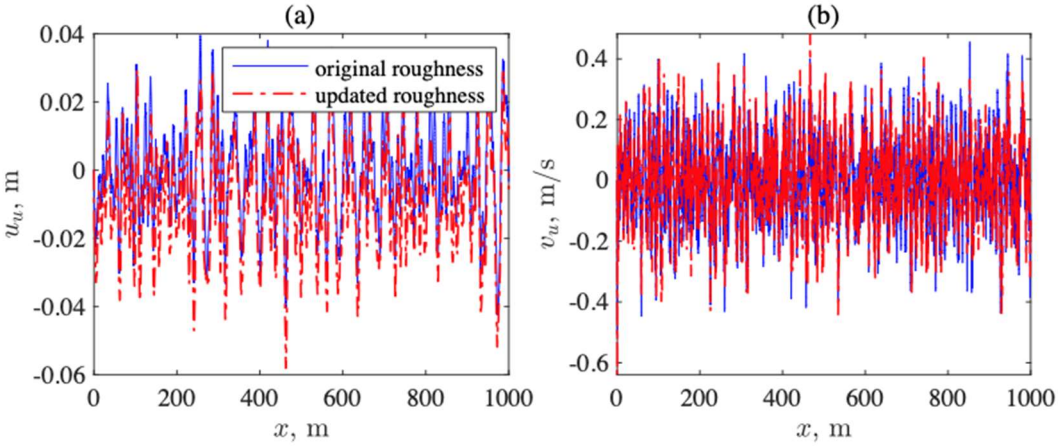

Figure 13. Comparison of vehicle responses before and after update. (a) displacement of the upsprung mass; (b) velocity of the unsprung mass.

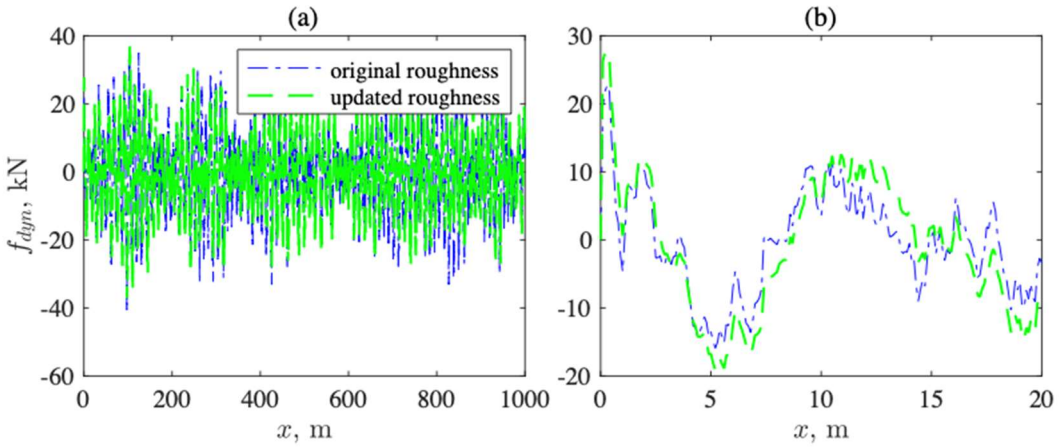

Figure 14. Comparison of dynamic interaction force before and after update. (a) results of the full 1000 m road section; (b) results of the road section of the first 20 m.

5.1.2. Case 2: Influence of Roughness Level

This subsection studies the influence of roughness level on the road surface deformation and the resultant vehicle dynamic loads. The vehicle traveling speed is v = 22.22 m/s. Six representative PSD values, i.e., $S_\xi(\kappa_0) = 2\times10^{-6}, 8\times10^{-6}, 32\times10^{-6}, 128\times10^{-6}, 512\times10^{-6}, 2048\times10^{-6}$ m^3/cycle that correspond to roughness classifications ranging from 'very good' to 'very poor' (Table 2) are used to evaluate the influence of roughness level on vehicle dynamic loads. Figures 15(a) to (f) illustrate the comparison of vehicle dynamic loads between the cases where the roughness deformation is ignored and cases where the roughness deformation is considered. We can find in Figures 15 (a) to (f) that the vehicle dynamic loads in the two cases are close, signaling that the roughness level has weak influence on the vehicle dynamic loads. To quantify the influence, Table 5 lists the amplification factor (ratio between the dynamic/total loads in the two cases) of the dynamic and total loads in the six roughness scenarios. It can be found that the dynamic amplification factor ranges from 0.95 to 1.06, and the total amplification factor ranges from 0.91 to 1.04.

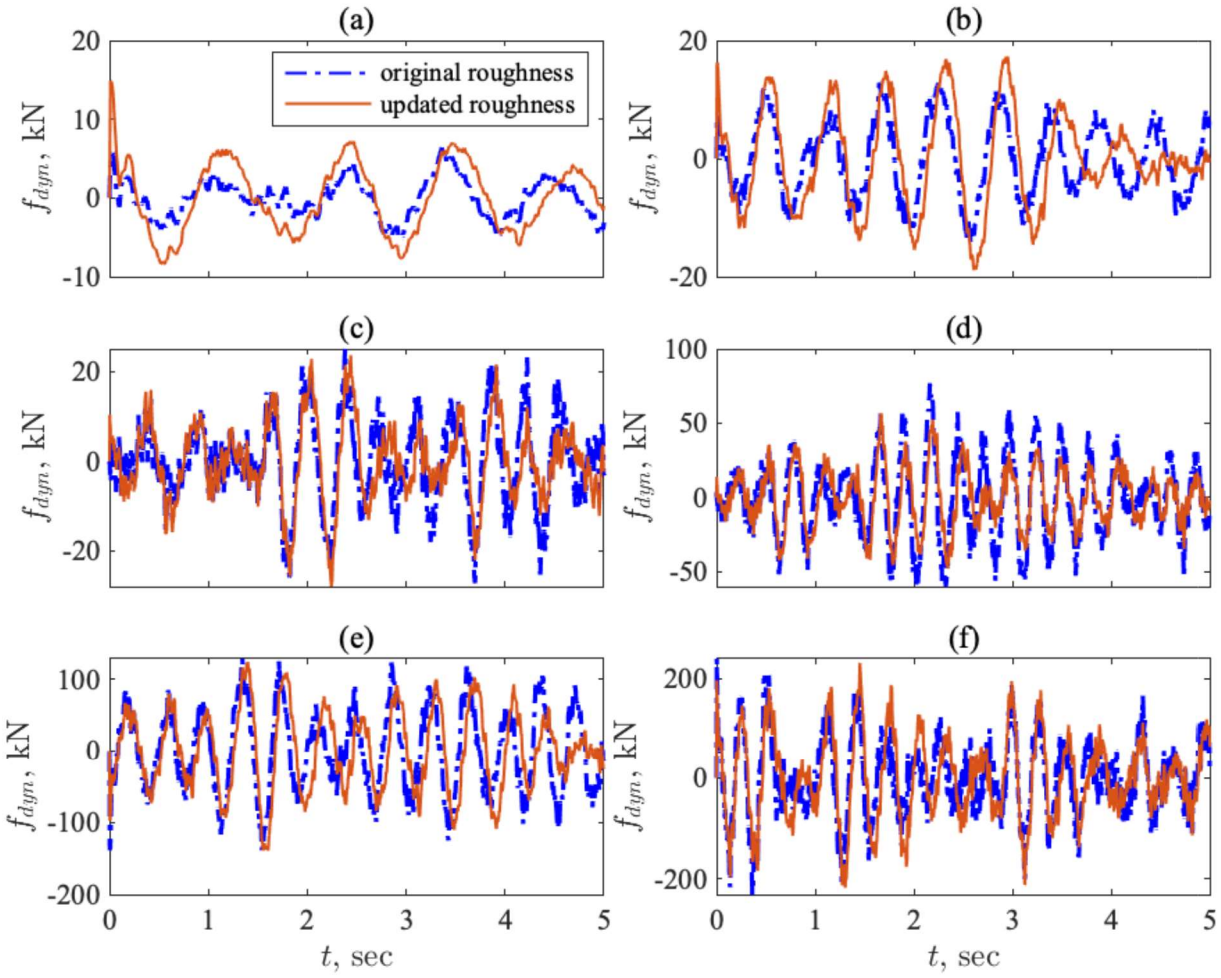

Figure 15. Dynamic interaction forces obtained at (a) $S_\xi(\kappa 0) = 2\times10\text{-}6$, (b) $S_\xi(\kappa 0) = 8\times10\text{-}6$, (c) $S_\xi(\kappa 0) = 3.2\times10\text{-}5$, (d) $S_\xi(\kappa 0) = 1.28\times10\text{-}4$, (d) $S_\xi(\kappa 0) = 5.12\times10\text{-}4$ and (e) $S_\xi(\kappa 0) = 2.048\times10\text{-}3$ m3/cycle.

Table 5. Amplification factor of interaction force.

$S_\xi(\kappa_0)$, 10^{-6} m^3/cycle	Dynamic interaction force	Overall interaction force
2	0.98	0.98
8	1.02	0.98
32	1.00	1.02
128	1.06	1.04
512	0.95	0.91
2048	1.01	1.03

5.1.3. Case 3: Influence of Vehicle Traveling Speed

This section investigates the influence of vehicle traveling speed on the vehicle-pavement interaction and the induced dynamic loads. The roughness level is set as $S_\xi(\kappa_0) = 3.2\times10^{-5}$ and the rear axle properties are used in this analysis. Figure 16 compares the updated roughness at different traveling speeds with the original roughness. It shows that the vehicle speed can significantly affect the road profile that the vehicle travels across, which thus changes the vehicle responses and the interaction forces between the vehicle and the pavement.

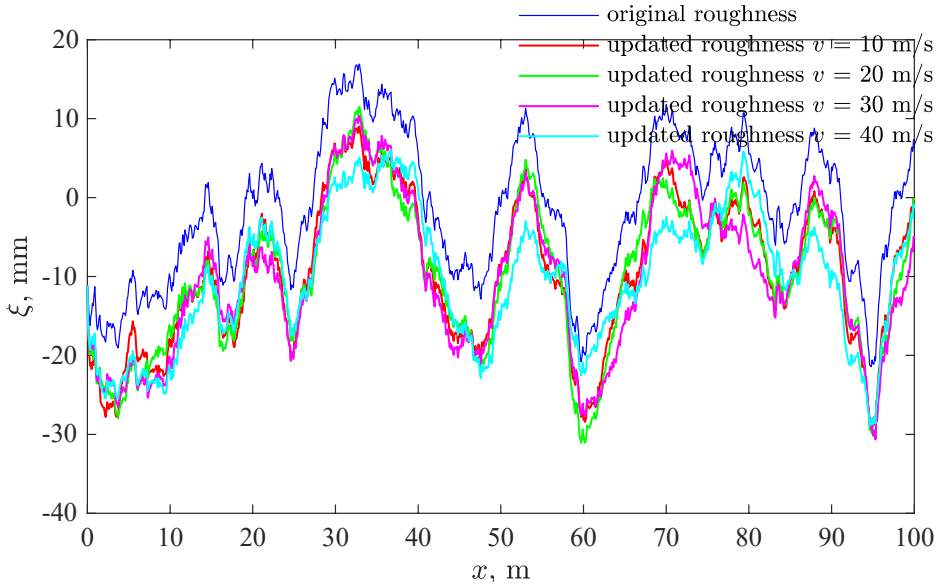

Figure 16. Comparison of updated roughness with original roughness at different vehicle speeds.

Figure 17 shows the updated dynamic interaction forces compared with the original results at different traveling speeds. The results of different traveling speeds are not directly comparable to each other because they correspond to identical locations. However, for the purpose of pavement analysis and design, an amplification factor of the interaction forces is valuable. Table 6 lists the amplification factor of the dynamic interaction force and overall interaction force (static plus dynamic interaction forces). We can find that the dynamic amplification factor varies between 0.71 and 1.31 under different traveling speeds, which should be considered when evaluating the dynamic loading effects, e.g., pavement fatigue analysis. Despite that the vehicle-pavement interaction causes considerable differences to the dynamic interaction force at different speeds, the influence on the overall interaction force is limited. As shown in the third column of Table 6, the total amplification factor ranges from 0.88 to 1.16. The changes of interaction forces are all below 20% (mostly below 5%) except for the cases with v = 35 m/s and v = 40 m/s. The mechanism for this difference is related to the vehicle dynamics and needs to be further investigated. It is possible that when the vehicle travels at a speed in the vicinity of the range from 35m/s to 40 m/s, the selected roughness input excites the resonant vibration of the quarter-car model and thus causes more significant changes to the vehicle induced dynamic and total loads on the pavements.

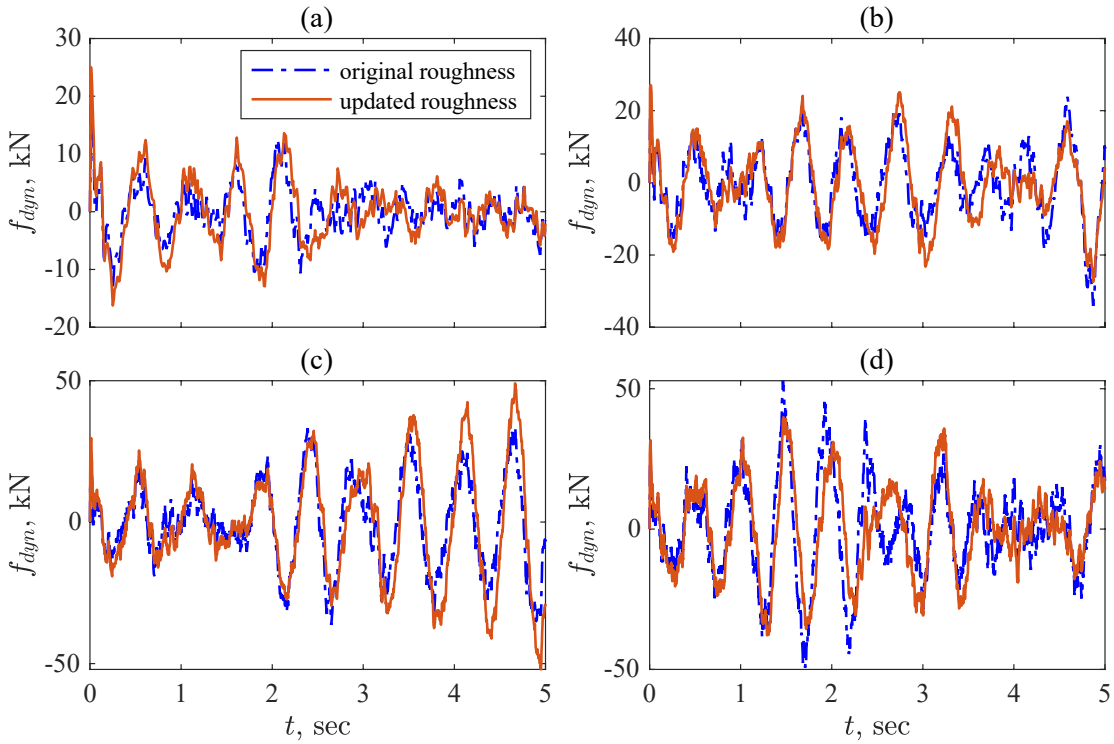

Figure 17. Dynamic interaction forces obtained at (a) v = 10 m/s; (b) v = 20 m/s; (c) v = 30 m/s; (d) v = 40 m/s.

Table 6. Amplification factor of interaction force.

Vehicle speed, m/s	Dynamic interaction force	Overall interaction force
5	1.13	1.03
10	0.93	1.01
15	1.01	1.00
20	0.88	0.98
25	0.95	0.97
30	1.11	1.06
35	1.31	1.16
40	0.71	0.88
45	1.15	1.04
50	0.97	1.00

5.2. Shakedown Limit Analysis without Considering the Vehicle-Road Couple Model

In this section, no consideration will be taken of the pavement roughness, which means that only $Q_{sta,unit}$ appears in the expression for the moving vehicle load, see Equation 7. Note that unless otherwise stated, the following values of $c_2 = 10$ kPa, φ_1=40°, and φ_2=30° are taken for the cohesion and frictional angle.

5.2.1. The Influence of Friction Coefficient/Friction Force

Friction force related to the friction coefficient between the tire and the pavement surface is an elementary factor to drive or brake vehicles. Their relationship can be expressed in a mathematical form which is shown as Equation 16b. If a truck is moving on the asphalt pavement, the friction coefficient is 0.008, which corresponds to the rolling friction coefficient. On the other hand, when the vehicle brakes this value will increase (from 0.008) to around 1, as the coefficient of rolling friction now switches to the sliding one.

The influence of the friction coefficient on the calculated shakedown limit is presented in Figure 18, where q_0 represents a unit moving stress on the pavement surface. It can be noted that the line pertaining to the case of rolling friction coefficient, i.e., $\upsilon = 0.008$, almost overlaps with the one without considering the friction force, which means that the influence of friction force on the shakedown limit can be ignored when a vehicle is moving on a pavement. In contrast, the shakedown limits become much lower in case of vehicle braking (i.e., $\upsilon = 0.5, 1$). It is clearly seen that the larger value of the cohesion ratio c_1/c_2, the more significant reduction of the shakedown limit with respect to the increase of the friction coefficient.

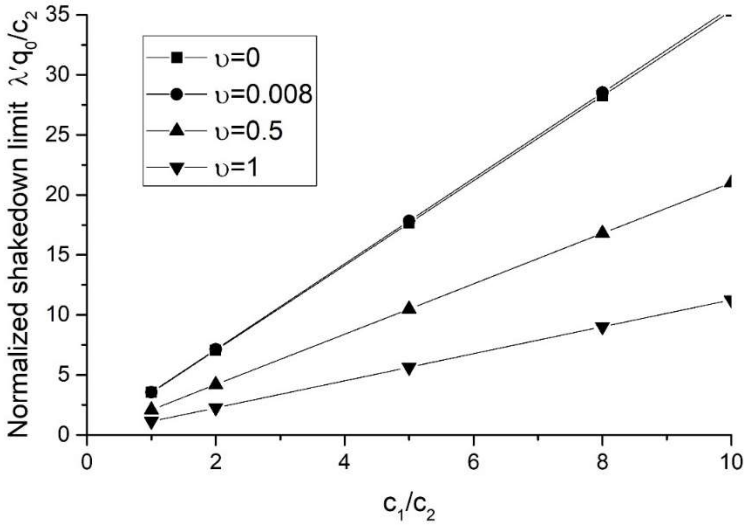

Figure 18. The influence of friction coefficient on the shakedown limit.

Since the friction force has negligible influence on the shakedown limit for a moving vehicle, it will not be involved in the following parametric analyses for the pavement shakedown limit.

5.2.2. The influence of Young's Modulus

Shakedown limits at various cohesion ratios are shown in Figure 19 (a) with different Young's modulus when the speed of a vehicle is 20 m/s. In this chart, it can be known that the shakedown

limit goes down with the rise of Young's modulus ratio E_1/E_2 at a relatively low cohesion ratio c_1/c_2=1, 2. It indicates that the critical point locates in the first layer. Its slope gradually decreases to zero after the E_1/E_2 over 10, which means that applying a high Young's modulus of the pavement layer does not have a significant effect on the shakedown limit. Whereas the shakedown limit climbs up with the growth of E_1/E_2 till reaches the peak value, and then gradually decreases with the climbing of E_1/E_2 at a relatively high cohesion ratio, e.g., c_1/c_2=5, 10. This shows that the location of the critical point has changed with the growing of Young's modulus ratio. It is in the second layer at a low E_1/E_2 (the increase part) and then moves to the first layer after the peak value (the decrease part). Actually, rising E_1/E_2 can achieve more stresses in the first layer. Consequently, the shakedown limit of the first layer will decrease with the rising of E_1/E_2. Whereas it increases the shakedown limit of the second layer. This is the reason which causes the change of the failure mode, and the shakedown limit keeps decrease while the stiffness of the first layer continually goes up.

The changing of normalized shakedown limit is proportional to the variation of c_1/c_2 if the critical point is in the pavement layer. For instance, when E_1/E_2 is fixed at 20 which is on the decrease part of the line in Figure 19 (a), the normalized shakedown limit is 5.6 if c_1/c_2=2, and it will increase proportionally to 22.4 with c_1/c_2 up to 8.

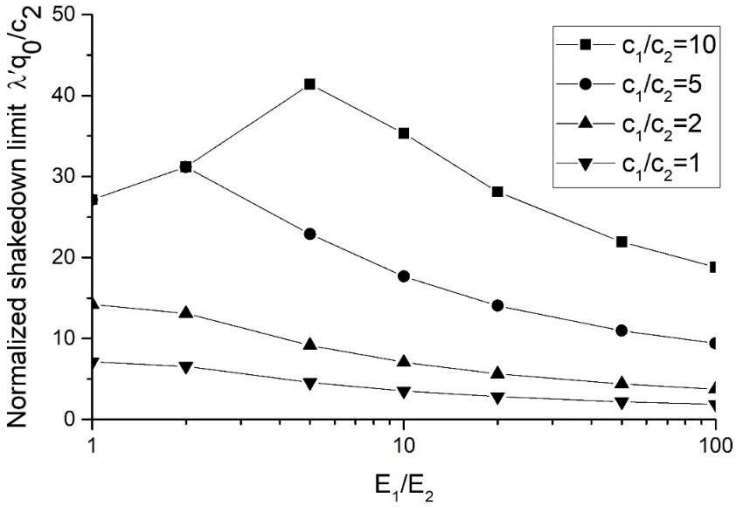

(a)

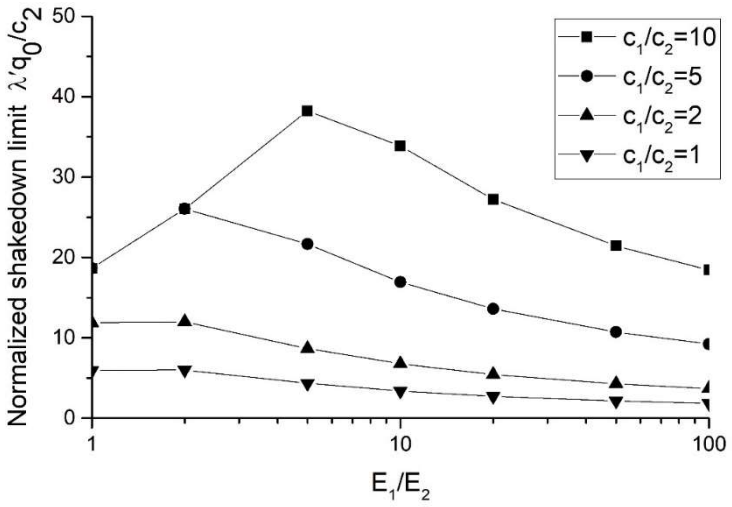

(b)

Figure 19. Influence of Young's modulus ratio to shakedown limit at various cohesion ratios (a) v=20 m/s and (b) v=45 m/s.

The shakedown limit $\lambda' q_0$ is non-dimensioned by the cohesion strength of the subsoil, c_2, so that the values in this chart can be widely used for various values of c_2 without re-computation. For example, based on the field observation, the maximum design traffic load is 1.6 MPa, and the cohesion strength of the subsoil is 50 kPa in the in-suit testing. The normalized shakedown limit $\lambda' q_0/c_2$ is 32. Consequently, it is easy to know that the minimum cohesion ratio c_1/c_2 should be 10 in this case since the maximum normalized shakedown limit is 31 if c_1/c_2 is not larger than 5.

However, in the above example, there are two values of E_1/E_2 that satisfy the designed maximum load if the chosen c_1/c_2 is 10, one is just over 2, the other one is around 17. It is recommended to choose the higher one, i.e., E_1/E_2=17, on the decrease part of the line. The reason is that stress and deformation should be as small as possible in the subsoil in the pavement design process. The critical point, on this point, should be in the pavement layer, which is easy for maintenance and repair during the pavement structure in the service stage.

Though the highest highway speed is 120 km/h in Louisiana and most of other states in the U. S. However, it is hard to supervise that every driver observes this instruction without speeding. To consider this phenomenon which may happen after the pavement construction, the velocity is speeded up to 45 m/s (162 km/h) which is a relatively high moving speed. The shakedown limits, in this case, are shown in Figure 19 (b). It provides a similar trend with the ones of 20 m/s at different cohesion ratios.

As shown in Figure 19, it should point out that the slope of the lines at a high cohesion ratio, i.e., c_1/c_2=5, 10, is larger than the one at a low c_1/c_2. Another significant feature is that there always exists an optimal E_1/E_2, i.e., the peak point on each line, which provides that largest shakedown limit. For example, if the moving speed is 20 m/s and the cohesion ratio equals 2, the optimal Young's modulus ratio is 1 since it is the largest one among various E_1/E_2 in this scenario. And it will increase to 5 if the c_1/c_2 jumps to 10.

Considering various friction angles of the upper layer, φ_1, shakedown limits are shown in Figure 20 (a) and (b). The cohesion strength of these two layers is the same, which is 10 kPa. The friction angle of the bottom layer is fixed at 30°. If the speed is 20 m/s, as shown in Figure 20 (a), all the lines fall off with the increasing of E_1/E_2 no matter what the value of the pavement friction angle. Their slopes gradually become smaller after E_1/E_2 over 10. This means that the critical point always exists in the first layer with varying of E_1/E_2 and φ_1. Different from the above one, when the velocity is 45 m/s which is shown in Figure 20 (b), shakedown limits on each line are almost stable when E_1/E_2 is not larger than 2 and then fall with the rise of E_1/E_2.

As we have known, both the cohesion strength, c, and the inner friction angle, φ, are two parameters that influence the material failure status in Mohr-Coulomb criteria. However, they show different effects on the shakedown limit though increase either of them has a positive influence on the shakedown limit. Compared Figures 19 (a) and 20 (a), or Figures 19 (b) and 20 (b), cohesion strength shows a stronger effect than the friction angle on the shakedown limit, even at a low E_1/E_2. For instance, when E_1/E_2 is 2 and the v is 20 m/s, the shakedown limit at c_1/c_2=2 is twice of the one at c_1/c_2=1, i.e., the increase ratio is 100%. Whereas the increase ratio is only 19.9% when the φ_1 increase from 30° to 40°. It is also easy to find that shakedown limits at different φ_1 almost convergent when the E_1/E_2 is over 50. Conversely, differences between ones at various c_1/c_2 are still obvious even E_1/E_2 =100. On the other hand, a high c_1/c_2 can change the failure mode which is caused by the critical shakedown point. But a high φ_1 does not show this phenomenon at a medium speed, $v = 20\ m/s$, and it only raises a slight increase in the φ_1 = 40° case at a relatively high vehicle velocity, $v = 45\ m/s$. These may indicate that cohesion ratio contributes more to the pavement system failure behavior.

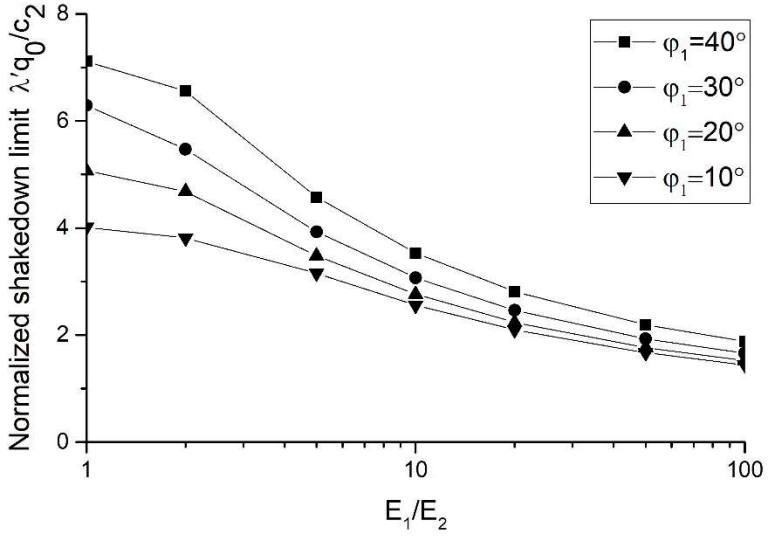

(a)

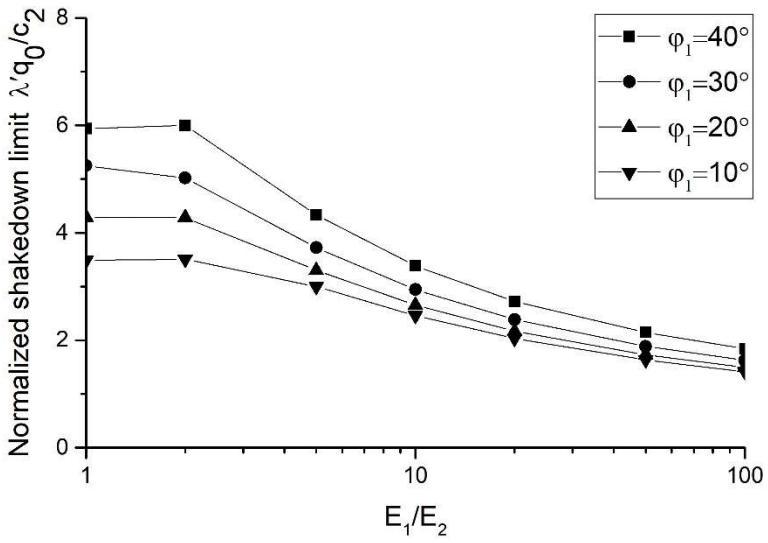

(b)

Figure 20. Influence of Young's modulus ratio to shakedown limit at various friction angles: (a) v=20 m/s and (b) v=45 m/s.

5.2.3. The influence of the Thickness of Pavement Layer

Figure 21 presents the shakedown limits at various thicknesses of the pavement layer. It is known that increasing the thickness has a positive effect on shakedown limits. But the shakedown limit will not continue to increase after the c_1/c_2 reaches a specific value in each scenario. For example, the shakedown limit stops to increase after c_1/c_2 over 15 when the h_1/a is 1. Increasing the cohesion strength of the first layer can improve the shear resistance so that it shows an increase in the shakedown limit. However, keeping an increase of c_1 gradually leads to that the critical point moves to the bottom layer and eventually the second layer becomes the critical layer in this pavement system, which is not what we hope to happen during the life-span of the pavement system.

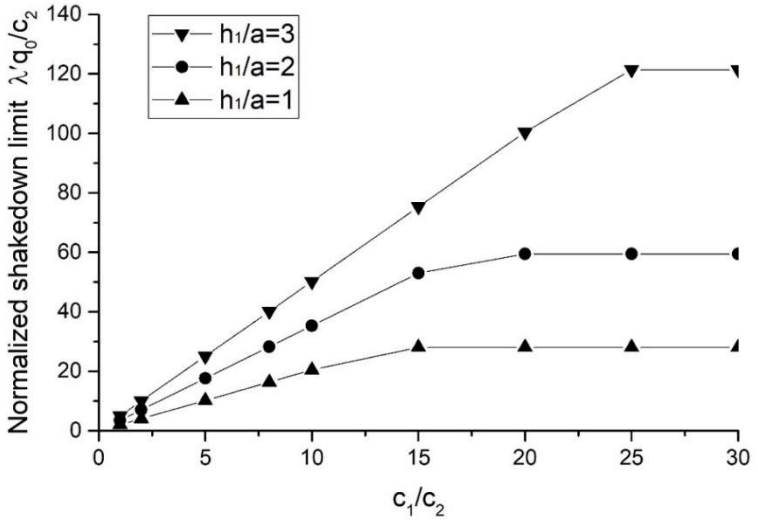

Figure 21. The influence of pavement thickness to shakedown limit.

5.2.4. The Influence of Velocity

The velocity is an important consideration in the progress of the design. It is noticed that different velocities can have unlike influence on the shakedown limit even if other parameters are the same in Figures 19 and 20.

Figure 22 (a) and (b) show shakedown limits at E_1/E_2=10 to consider the influence of changing velocities at various cohesion ratios c_1/c_2 and friction angles of the pavement layer, φ_1, respectively. In Figure 22 (a), friction angles in each layer of the pavement system are the same, which is 30°, and the cohesion strength c_2 is 10 kPa. When the cohesion strength of the pavement layer is not too stronger than the one of the subsoil, for instance, c_1/c_2=1 or 2, increasing speed has no influence on the shakedown limit. But it slightly goes down with speeding up for high cohesion strength of the pavement layer, i.e., c_1/c_2=5 or 10. To consider the influence of velocities at different pavement friction angles, φ_1, cohesion strength of the pavement system is fixed at 10 kPa, and the φ_2 is 30°. The results are presented in Figure 22 (b). Compared with (a), it shows a similar downward trend, but its slope is steeper than the ones at various c_1/c_2. However, the decrease ratio of shakedown limit is small. For example, it is only 0.09 when the speed increases to 60 m/s from 10 m/s in the case of φ_1 = 40°.

Based on Qian et al. *(58)*'s results, the shakedown limit gradually decreases till the Rayleigh wave speed, and the lower ratio of the moving speed over the Rayleigh wave speed raises a larger shakedown limit at a specific stiffness modulus. Rayleigh speed increases with the growth of Young's modulus in a layered system *(83)*. The Rayleigh wave speed can be expressed as follows according to *(73)*,

$$c_R = \frac{0.862+1.14\nu}{1+\nu} c_s \quad [22a]$$

$$c_s = \sqrt{\frac{\mu}{\rho}} \quad [22b]$$

where:

c_R, c_s= the Rayleigh and shear wave speed, respectively.

The Rayleigh wave speed is 291 m/s since $E_1 = 500\ MPa$ in this example. The ratio of the moving load at 60 m/s over the Rayleigh wave speed is 0.21. Though the velocity is relatively high, it is still comparatively small with the Rayleigh wave speed that is the lowest shakedown limit. Thus, the shakedown limit does not show a significant drop off with the rise of velocity.

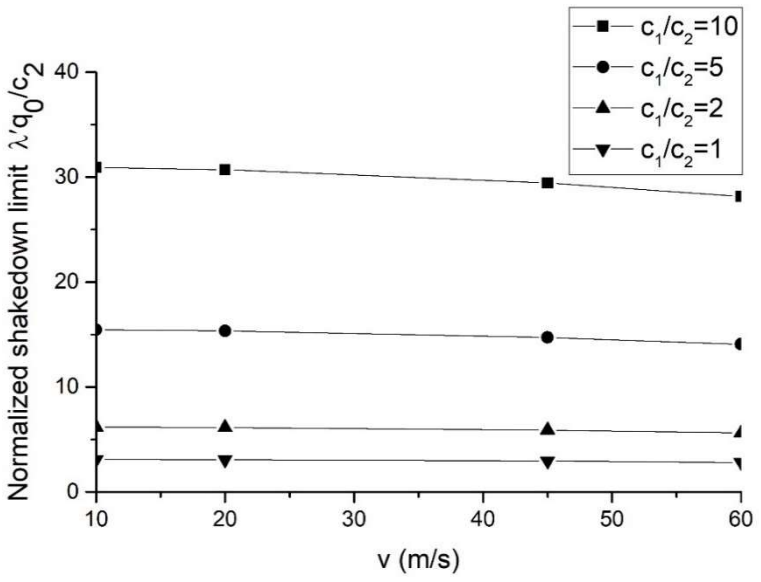

(a)

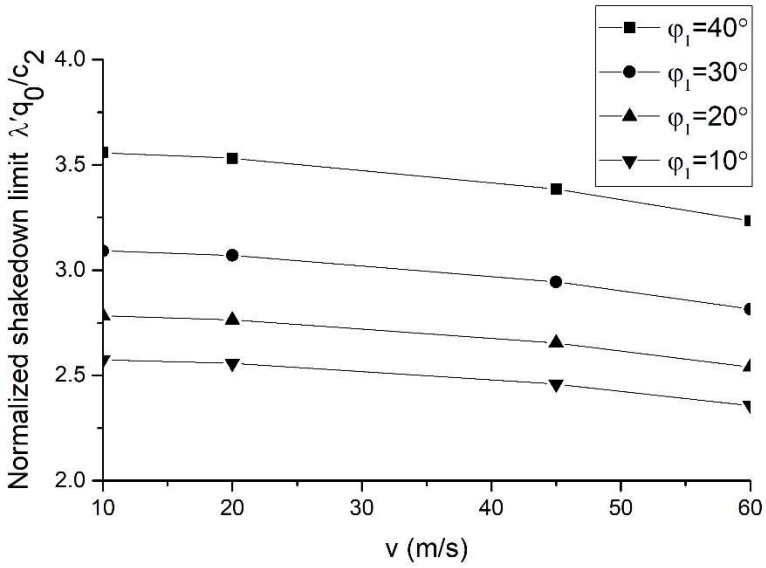

(b)

Figure 22. The influence of velocities of the moving load to shakedown limit: (a) various c_1/c_2 and (b) various φ_1.

5.2.5. The Shakedown Limit in a Three-layered Pavement System

In practical engineering, a pavement system consists of many layers with different material properties. A three-layered pavement structure consisting of a hot mix asphalt (HMA) layer, a granular base, and a subsoil half-infinite layer from the top to the bottom is considered in this subsection to analyze the influence of cohesion ratio on the shakedown limit.

Properties of HMA are strongly affected by the temperature. Especially in Louisiana, the temperature of the ground surface may approach 50°C at noon in the summer. Thus, we consider two Young's modulus of the asphalt in different scenarios, one is at 49°C which represents the

noon case, and the other one is at 21°C which is the night case. Material properties are shown in Table 7 and the results of the shakedown limit are shown in Figures 23 and 24.

Table 7. Material properties in a three-layer pavement system.

Layer	Young's modulus E (MPa)	Poisson's Ratio ν	Density ρ(kg/m^3)	Cohesion c (kPa)	Internal friction angle φ (°)
1(HMA Layer)	3500 (21°C) 150 (49°C)	0.25	2000	30-300	10
2(Granular Base)	300	0.25	2000	30-300	10
3(Subsoil)	50	0.25	2000	10	30

The shakedown limit with various c_1/c_2 in the noon case is depicted in Figure 23. Since the modulus of asphalt drops dramatically because of the high temperature, Young's modulus of the second layer changes to the largest one in this case. Based on the previous analysis for a two-layered pavement system, an increase in the cohesion strength can raise the shakedown limit of the pavement system. However, from Figure 23 (a) it seems that increasing c_1 does not have any contributions to the shakedown limit of the whole pavement system. Note that in this chart, to explore the influence of c_1, a fixed value of $c_2 = 30$ kPa has been used throughout the numerical analysis. It is easy to find that the system shakedown, which is represented by the red solid line, keeps at a value with the rise of c_1/c_2 and overlaps with the blue dash line, which represents the second layer, i.e., the granular layer, shakedown limit. The green dash line represents the shakedown limit of the HMA layer. It clearly shows that the shakedown limit of the HMA layer has a dramatic increase with the increase of c_1/c_2. However, it is above the ones of the second layer from the beginning to the end. It indicates that the second layer is the critical one in this system based on Equation 21. The reason is the stiffness modulus of the granular layer is the largest among this three-layer structure, so it yields the most stresses in this layer and presents as a control layer.

However, the result is not the same as the above one by changing the c_2. As the red solid line is shown in Figure 23 (b) when c_1 is 30 kPa, the system shakedown limit increases with the rise of c_2/c_1 before approaching a specific value. The green and blue dash lines represent the shakedown limit in the first and second layers, respectively. The shakedown limit of the second layer increases with the climbing of c_2/c_1, and an intersection point can be found at c_2/c_1= 5. It means that the second layer shakedown limit will larger than the first one and the failure mode of the pavement will be transformed from the second layer failure to the first layer after this point. It is easy to maintain and rebuild if the failure happens in the uppermost layer. Thus, for the noon scenario, it is recommended to increase the cohesion strength of the second rather than the one in the first layer.

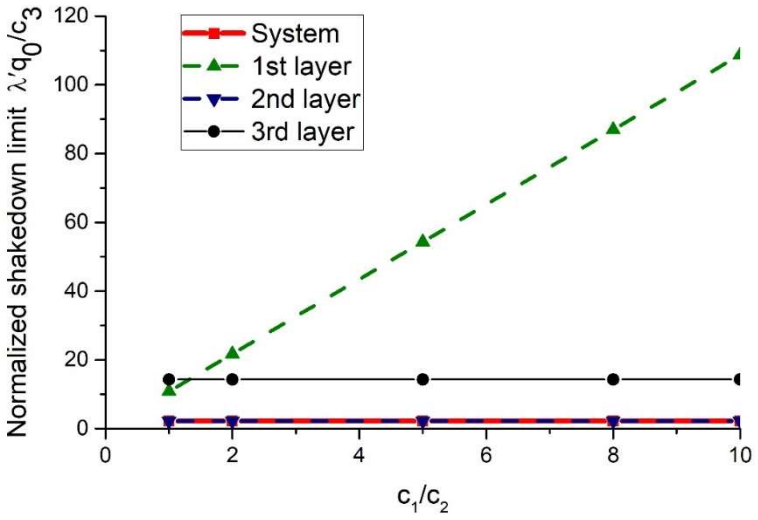

(a)

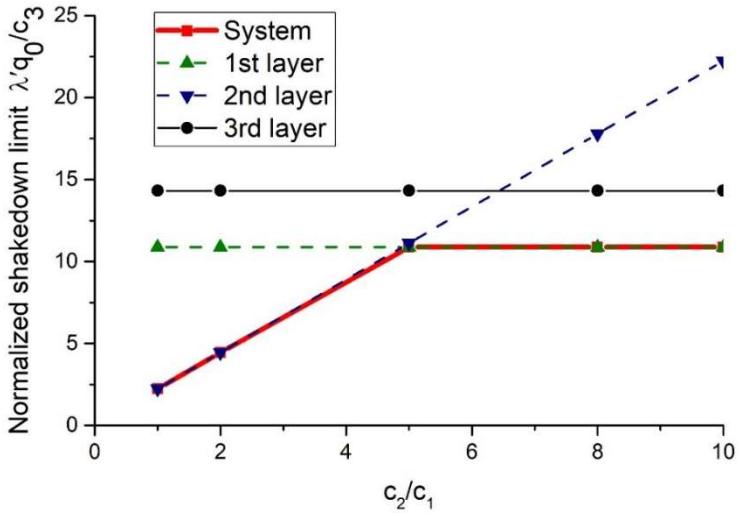

(b)

Figure 23. Shakedown limit in a three-layer pavement system in a noon case: (a) increasing c_1/c_2 and (b) increasing c_2/c_1.

At a relatively low temperature, Young's modulus of HMA presents a high value. Figure 24 depicts the shakedown limits of the pavement system and each layer with various c_1/c_2. It shows a similar result with the two-layer case. The shakedown limit of the system is controlled by the MHA layer if the c_1/c_2 is smaller than a specific value, as shown by the overlap between the red solid line and the green dash line before c_1/c_2 reaches 8 in Figure 24. But the critical point will move to the second layer since the high c_1/c_2 gradually increase the ability to resist the shear failure in the first layer.

Therefore, based on the results shown in Figures 23 and 24, it is important to place the high stiffness modulus layer over the lower modulus one because the layer with the largest Young's modulus predominates the failure mode of the pavement structure at a low c_1/c_2. However, if layers cannot be placed by means of a monotonically decreasing stiffness modulus, it may be a

good method to appropriately increase the cohesion strength of the layer in which has the largest stiffness modulus among all layers.

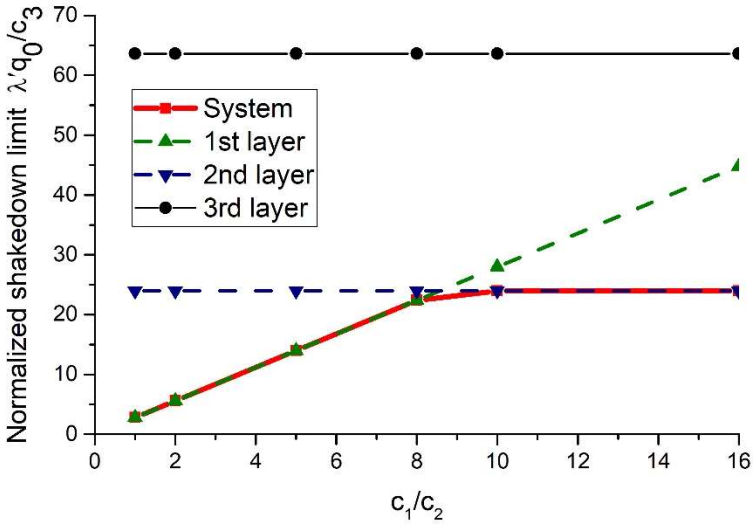

Figure 24. Shakedown limit in a three-layer pavement system in a night case.

5.3. The Shakedown Limit Analysis Incorporating the Vehicle-Road Couple Model

As discussed in 5.1., the total amplification factor ranges from 0.88 to 1.16 under different traveling speeds. To simplified it when considering the influence on the shakedown limit, the total amplification factor is chosen as 0.8, 0.9, 1.0, 1.1, and 1.2. A two-layer pavement structure is chosen as an illustration example, in which the material properties employed are c_1/c_2 = 5, c_2 = 10 kPa, φ_1 = 40°, and φ_1 = 30°. As shown in Figure 25, a larger amplification factor results in a lower shakedown limit for all the modulus ratio of E_1/E_2 ranging from 1 to 100, which is as expected. The reason is that an amplification factor that is over 1 can increase stress fields in the pavement system and lead to a decrease in the maximum load to ensure the system in shakedown status. Further study on the shakedown limit under the amplification, we can find that the shakedown limit is inversely proportional to the amplification. For example, when E_1/E_2 equals 2, the normalized shakedown limit is 22.88 for the factor at 1. It drops to 19.07 when the factor grows up to 1.2. The ratio of the shakedown limits is 0.83 which approaches 1/1.2. This indicates that the amplification may not be considered during the solving process of the shakedown limit for a pavement structure. This is because for a given pavement structure, the shakedown limit is not related to the load amplitude, increasing the applied load can only accelerate stress fields to the yield or failure status. Therefore, it only needs to be considered when determining the maximum design load. For instance, if the maximum is 50 kPa without involving the influence of the pavement roughness, it should be decreased to 41.67 kPa if the amplification factor is 1.2 when using the line without roughness effect, i.e., the line with circle symbol in Figure 25.

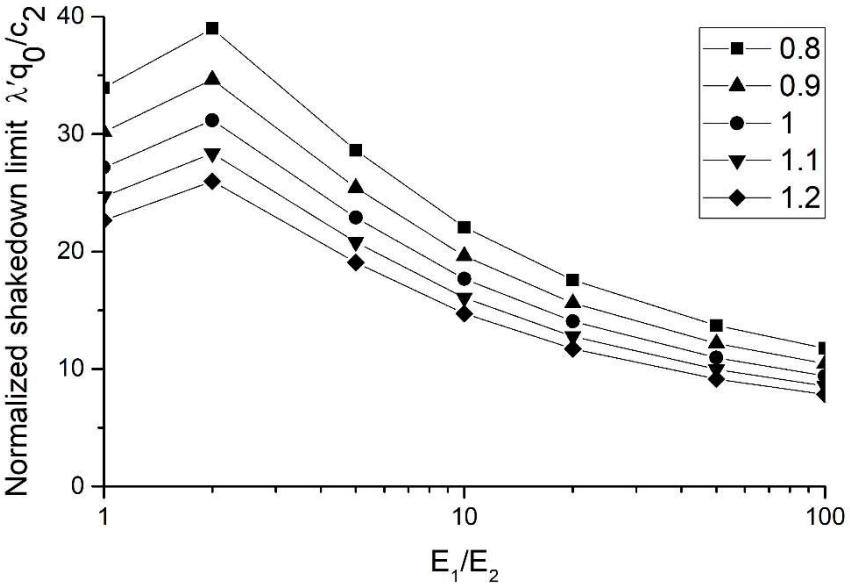

Figure 25. The influence of the pavement roughness on the shakedown limit.

6. CONCLUSIONS

This research project develops an advanced model for the pavement performance assessment, using the plasticity-based shakedown theory. The work has been focused on the understanding of vehicle road interaction and the stress characteristics of pavement system under moving surface loads, and in particular on the development of a Matlab framework for evaluating the critical shakedown load. The proposed shakedown approach, given its ability to cope with the pavement roughness and the dynamic effects induced by the vehicle loads, would be an improvement over the existing analysis/design methodologies such as the empirical method and mechanistic-empirical method. According to the analytical modelling and numerical results from the developed vehicle-road coupling model and the shakedown analysis framework, the following major conclusions can be drawn:

1) At the traveling velocity $v = 22.22$ m/s which is used to determine IRI, the road profile is shifted downward by a certain amount while the road roughness has slight changes. As a result, the vehicle induced dynamic loads vary slightly (around 4%).

2) When different representative roughness levels are considered, the vehicle-induced dynamic amplification factor ranges from 0.95 to 1.06, and the total amplification factor ranges from 0.91 to 1.04. To the contrary, the amplification factor varies between 0.71 and 1.31 under different traveling speeds. This needs to be considered when evaluating the dynamic loading effects, e.g., pavement fatigue analysis. In addition, the total amplification factor ranges from 0.88 to 1.16 under different traveling speeds.

3) Numerical analyses for the case of two-layered flexible pavement indicates that there generally exists an optimal Young's modulus ratio between the pavement and subsoil, for which a maximum shakedown load of the pavement system will be reached when the other parameters remain unchanged. The influence of rolling friction force can be ignored for a moving vehicle, nevertheless it could become significant during the braking process as a result of the exerted slipping friction force in this scenario.

4) In general, the calculated shakedown limit of the pavement will increase with the pavement cohesion strength and internal friction angle, and with the pavement thickness as well. For the typical pavement-base-subsoil system, it is recommended that the three layers be such arranged/designed that their respective stiffness modulus decreases monotonically with the depth, to achieve the maximum value of the pavement shakedown limit. Alternatively, an appropriate adjustment/increase of the Young's modulus in the middle layer of the pavement system may also contribute to an increase in the critical shakedown load of the pavement system.

5) The shakedown limit shows an inverse proportional relationship with the amplification factor introduced by the vehicle-road couple model. The amplification factor needs only to be considered in the determination/design of the maximum traffic load.

REFERENCES

1. Dodds, C. J., & Robson, J. D. (1973). The Description of Road Surface Roughness. *Journal of sound and vibration*, 31(2), 175-183.

2. Hardy, M. S. A., & Cebon, D. Importance of Speed and Frequency in Flexible Pavement Response. *Journal of Engineering Mechanics*, 1994, 120(3), 463-482.

3. Iyengar, R. N., & Jaiswal, O. R. Random Field Modeling of Railway Track Irregularities. *Journal of Transportation Engineering*, 1995, 121(4), 303-308.

4. Sun, L., Deng, X. Predicting Vertical Dynamic Loads Caused by Vehicle-Pavement Interaction, *Journal of Transportation Engineering*, 1998, 124(5): 470-478

5. Qian, J., Zhou, R., Chen, S., Gu, X., & Huang, M. Influence of Pavement Roughness on Dynamic Stresses in Saturated Subsoil Subjected to Moving Traffic Loading. *International Journal of Geomechanics*, 2018, 18(4), 04018012.

6. Collins, I. F., and M. Boulbibane. Geomechanical Analysis of Unbound Pavements Based on Shakedown Theory. *Journal of Geotechnical and Geoenvironmental Engineering*, 2000, 126, No. 1, 50–59.

7. American Association of State and Highway Transportation Officials. *AASHTO Guide for Design of Pavement Structures*. Washington D.C., 1993.

8. Nguyen, A. D., Hachemi, A., & Weichert, D. Application of the Interior-Point Method to Shakedown Analysis of Pavements. *International Journal for Numerical Methods in Engineering*, 2008, 75(4), 414-439.

9. Yu, H. S. Three-Dimensional Analytical Solutions for Shakedown of Cohesive-Frictional Materials Under Moving Surface Loads. *Proceedings of the Royal Society A: Mathematical, Physical and Engineering Sciences*, 2005, 461(2059), 1951-1964.

10. Yu, H. S., and Wang, J. Three-Dimensional Shakedown Solutions for Cohesive-Frictional Materials Under Moving Surface Loads. *International Journal of Solids and Structures*, 2012, 49(26), 3797-3807.

11. Zhuang, Y., and Wang, K. Shakedown Solutions for Pavement Structures with von Mises Criterion Subjected to Hertz Loads. *Road Materials and Pavement Design*, 2018, 19(3), 710–726.

12. Boulbibane, M., and Ponter, A. R. S. The Linear Matching Method for the Shakedown Analysis of Geotechnical Problems. *International Journal for numerical and analytical methods in geomechanics*, 2006, 30(2), 157-179.

13. Chen, H. F., & Ponter, A. R. On the Behaviour of a Particulate Metal Matrix Composite Subjected to Cyclic Temperature and Constant Stress. *Computational materials science*, 2005, 34(4), 425-441.

14. Raad, L., and Minassian, G. The Influence of Granular Base Characteristics on Upper Bound Shakedown of Pavement Structures. *Road Materials and Pavement Design*, 2005, 6(1), 53–79.

15. Ghadimi, B., Nikraz, H., and Rosano, M. Dynamic Simulation of a Flexible Pavement Layers Considering Shakedown Effects and Soil-Asphalt Interaction. *Transportation Geotechnics*, 2016, 7, 40–58.

16. Boulbibane, M., and Ponter, A. R. S. Linear Matching Method for Limit Load Problems Using the Drucker–Prager Yield Condition. *Géotechnique*, 2005, 55(10), 731-739.

17. Yu, H. S. *Plasticity and Geotechnics (Vol. 13)*. Springer Science & Business Media, New York, 2007.

18. Kachanov, L. M. *Foundations of the Theory of Plasticity (Vol. 12)*. North-Holland, 1971.

19. Koiter, W. T. General Theorems for Elastic Plastic Solids. *Progress of Solid Mechanics*, 1960, 167-221.

20. Melan E. Der Der Spannungszustand eines Hencky-Mises'schen Kontinuums bei veranderlicher Belastung. *Sitzungberichte der Ak Wissenschaften Wien (Ser 2A)*, 1938, 147:73.

21. König, J. A. *Shakedown of Elastic-Plastic Structures*. Elsevier, Amsterdam, 2012.

22. Yu, H. S., Wang, J., and Liu, S. Three-Dimensional Shakedown Solutions for Cross-Anisotropic Cohesive-Frictional Materials Under Moving Loads. *Direct methods for limit and shakedown analysis of structures*, 2015, Springer, Cham. pp. 299-313.

23. Zarka, J. Direct Analysis of Elastic–Plastic Structures With 'Overlay' Materials during Cyclic Loading. *International Journal for Numerical Methods in Engineering*, 1980, 15(2), 225-235.

24. Stein, E., Zhang, G., and König, J. A. Shakedown with Nonlinear Strain-Hardening including Structural Computation using Finite Element Method. *International Journal of Plasticity*, 1992, 8(1), 1-31.

25. Pycko, S., and Maier, G. Shakedown Theorems for Some Classes of Nonassociative Hardening Elastic-Plastic Material Models. *International Journal of Plasticity*, 1995, 11(4), 367-395.

26. Chinh, P. D. Shakedown Theory for Elastic Plastic Kinematic Hardening Bodies. *International Journal of Plasticity*, 2007, 23(7), 1240-1259.

27. Polizzotto, C. Shakedown Analysis for a Class of Strengthening Materials within the Framework of Gradient Plasticity. *International journal of plasticity*, 2010, 26(7), 1050-1069.

28. Chen, H., and Ponter, A. R. A Simplified Creep-Reverse Plasticity Solution Method for Bodies Subjected to Cyclic Loading. *European Journal of Mechanics-A/Solids*, 2004, 23(4), 561-577.

29. Klebanov, J. M., and Boyle, J. T. Shakedown of Creeping Structures. *International journal of solids and structures*, 1998, 35(23), 3121-3133.

30. Peigney, M. Shakedown of Elastic-Perfectly Plastic Materials with Temperature-Dependent Elastic Moduli. *Journal of the Mechanics and Physics of Solids*, 2014, 71, 112-131.

31. Sharp, R. W. *Shakedown Analysis and Design of Pavements*, 1983.

32. Sharp, R. W., and Booker, J. R. Shakedown of pavements under moving surface loads. *Journal of Transportation Engineering*, 1984, 110(1), 1-14.

33. Collins, I. F., and Cliffe, P. F. Shakedown in Frictional Materials under Moving Surface Loads. *International Journal for Numerical and Analytical Methods in Geomechanics*, 1987, 11(4), 409-420.

34. Radovsky, B. S., and Murashina, N. V. Shakedown of Subgrade Soil under Repeated Loading. *Transportation Research Record*, 1996, 1547(1), 82-88.

35. Shiau, S. H., and Yu, H. S. Load and Displacement Prediction for Shakedown Analysis Of Layered Pavements. *Transportation Research Record*, 2000, 1730(1), 117-124.

36. Krabbenhøft, K., Lyamin, A. V., and Sloan, S. W. Shakedown of a Cohesive-Frictional Half-Space Subjected to Rolling and Sliding Contact. *International Journal of Solids and Structures*, 2007, 44(11-12), 3998-4008.

37. Werkmeister, S., Dawson, A. R., and Wellner, F. Permanent Deformation Behavior of Granular Materials and the Shakedown Concept. *Transportation Research Record*, 2001, 1757(1), 75-81.

38. Werkmeister, S., Dawson, A. R., and Wellner, F. Pavement Design Model for Unbound Granular Materials. *Journal of Transportation Engineering*, 2004, 130(5), 665-674.

39. Werkmeister, S., Dawson, A. R., and Wellner, F. Permanent Deformation Behaviour of Granular Materials. *Road Materials and Pavement Design*, 2005, 6(1), 31-51.

40. Sangrey, D. A., Henkel, D. J., and Esrig, M. I. The Effective Stress Response of a Saturated Clay Soil to Repeated Loading. *Canadian Geotechnical Journal*, 1969, 6(3), 241-252.

41. Muhanna, A. S., Rahman, M. S., and Lambe, P. C. Model for Resilient Modulus and Permanent Strain of Subgrade Soils. *Transportation Research Record*, 1998, 1619(1), 85-93.

42. Yang, S. R., and Huang, W. H. Permanent Deformation and Critical Stress of Cohesive Soil under Repeated Loading. *Transportation research record, 2007*, 2016(1), 23-30.

43. Sharp, R. W. Pavement Design Based on Shakedown Analysis. *Transportation Research Record*, 1985, 1022(99), 107.

44. Brett, J. F. Stability and Shakedown in Pavement Roughness Change with Age. *New Zealand Roading Symposium*, 1987, Wellington, New Zealand, volume 4, pp: 695-704.

45. Allou, F., Petit, C., Chazallon, C., and Hornych, P. Shakedown Approaches to Rut Depth Prediction in Low-Volume Roads. *Journal of Engineering Mechanics*, 2010, 136(11), 1422-1434.

46. Ahmad, J., Rahman, M. A., and Hainin, M. R. Rutting Evaluation of Dense Graded Hot Mix Asphalt Mixture. *International Journal of Engineering & Technology (IJET-IJEN)*, 2011, 11(05), 56-60.

47. Liu, S., Wang, J., Yu, H. S., Wanatowski, D., Thom, N., and Grenfell, J. Shakedown of Asphalt Pavements Considering Temperature Effect. *International Journal of Pavement Engineering*, 2020, 1-12.

48. Raad, L., Weichert, D., and Najm, W. Stability of Multilayer Systems under Repeated Loads. *Transportation Research Record*, 1988, 1207, pp: 181-186.

49. Raad, L., Weichert, D., and Haidar, A. Analysis of Full-Depth Asphalt Concrete Pavements using Shakedown Theory. *Transportation Research Record*, 1989, 1227, 53-65.

50. Najm, W. A. S. *Numerical Application of Shakedown Theory to Multilayer Systems*, 1987, Doctoral dissertation, American University of Beirut.

51. Raad, L., Weichert, D., and Haidar, A. Shakedown and Fatigue of Pavements with Granular Bases. *Transportation Research Record*, 1998, 1227, pp: 159-172.

52. Yu, H. S., and Hossain, M. Z. Lower Bound Shakedown Analysis of Layered Pavements using Discontinuous Stress Fields. *Computer Methods in Applied Mechanics and Engineering*, 1998, 167(3-4), 209-222.

53. Liu, S. *Application of Shakedown Theory in the Structural Design of Bituminous Pavements*, 2016, Doctoral dissertation, University of Nottingham.

54. Ponter, A. R. S., Hearle, A. D., & Johnson, K. L. Application of the Kinematical Shakedown Theorem to Rolling and Sliding Point Contacts. *Journal of the Mechanics and Physics of Solids*, 1985, 33(4), 339-362.

55. Chen, S., Liu, Y., and Cen, Z. Lower Bound Shakedown Analysis by using the Element Free Galerkin Method and Non-Linear Programming. *Computer Methods in Applied Mechanics and Engineering*, 2008， 197(45-48), 3911-3921.

56. Wang, J., and Yu, H. S. Shakedown Analysis for Design of Flexible Pavements under Moving Loads. *Road Materials and Pavement Design*, 2013, 14(3), 703-722.

57. Wang, J., & Yu, H. S. Three‐Dimensional Shakedown Solutions for Anisotropic Cohesive‐Frictional Materials under Moving Surface Loads. *International Journal for Numerical and Analytical Methods in Geomechanics*, 2014, 38(4), 331-348.

58. Qian, J., Wang, Y., Lin, Z., Liu, Y., and Su, T. Dynamic Shakedown Analysis of Flexible Pavement under Traffic Moving Loading. *Procedia Engineering*, 2016, 143, 1293-1300.

59. Collins, I. F., Wang, A. P., and Saunders, L. R. Shakedown in Layered Pavements under Moving Surface Loads. *International Journal for Numerical and Analytical Methods in Geomechanics*, 1993, 17(3), 165-174.

60. Ponter, A. R., and Engelhardt, M. Shakedown Limits for a General Yield Condition: Implementation and Application for a von Mises Yield Condition. *European Journal of Mechanics-A/Solids*, 2000, 19(3), 423-445.

61. Huang, M., and Yao, Z. Analysis of Traffic-Load-Induced Permanent Settlement of Highway Embankment on Soft Clay Ground. *2nd International Conference on Transportation Geotechnics (ICTG)* International Society of Soil Mechanics and Geotechnical Engineering (ISSMGE), 2012, London, 110-117.

62. Qian, J., Zhang, J. F., Wang, Y., and Ma, X. An Equivalent Finite Element Method for Traffic-Load-Induced Settlement of Pavement on the Soft Clay Subgrade. *Computer Methods and Recent Advances in Geomechanics: Proceedings of the 14th International Conference of International*

Association for Computer Methods and Recent Advances in Geomechanics, 2014 (IACMAG 2014), 2015, Taylor & Francis Books Ltd., London, 1835-1840.

63. Cai, Y., Wu, T., Guo, L., and Wang, J. Stiffness Degradation and Plastic Strain Accumulation of Clay under Cyclic Load with Principal Stress Rotation and Deviatoric Stress Variation. *Journal of Geotechnical and Geoenvironmental Engineering*, 2018, 144(5), 04018021.

64. Qian, J., Zhou, R., Chen, S., Gu, X., & Huang, M. Influence of Pavement Roughness on Dynamic Stresses in Saturated Subsoil Subjected to Moving Traffic Loading. *International Journal of Geomechanics*, 2018, 18(4), 04018012.

65. Huang, Y. H. *Pavement Analysis and Design, 2nd Ed.*, Pearson Prentice Hall, Upper Saddle River, N.J., 2004.

66. Chazallon, C., Koval, G., Hornych, P., Allou, F., & Mouhoubi, S. Modelling of Rutting of Two Flexible Pavements with the Shakedown Theory and the Finite Element Method. *Computers and Geotechnics*, 2009, 36(5), 798-809.

67. Wu, Jiunn-Jong. Simulation of Rough Surfaces with FFT. *Tribology International,* 33.1, 2000: 47-58.

68. Jiang, C. D., Cheng, L., Fengchun, S., & Hongjie, C. Simulation of Road Roughness Based on using IFFT Method. *2012 Third World Congress on Software Engineering*, 2012, IEEE, pp. 190-193.

69. Bender, Carl M., and Steven A. Orszag. *Advanced Mathematical Methods for Scientists and Engineers I: Asymptotic Methods and Perturbation Theory*. Springer Science & Business Media, 2013.

70. Andren, Peter. Power Spectral Density Approximations of Longitudinal Road Profiles. *International Journal of Vehicle Design,* 40.1-3, 2006: 2-14.

71. Cebon, David. *Handbook of Vehicle-Road Interaction*. 1999.

72. Sayers, M., and Karamihas S. *The Little Book of Profiling: Basic Information About Measuring and Interpreting Road Profiles*. University of Michigan. Transportation Research Institute, UMTRI, 1996.

73. Achenbach, J. *Wave Propagation in Elastic Solids*. North-Holland Publishing Company, New York, NY, 1973.

74. Maina, J. W., Ozawa, Y., & Matsui, K. Linear Elastic Analysis of Pavement Structure under Non-Circular Loading. *Road Materials and Pavement Design*, 2012, 13(3), 403-421.

75. Jones, D. V., Le Houedec, D., Peplow, A. T., & Petyt, M. Ground Vibration in the Vicinity of a Moving Harmonic Rectangular Load on a Half-Space. *European Journal of Mechanics-A/Solids*, 1998, 17(1), 153-166.

76. Harkrider, D. G. Surface Waves in Multilayered Elastic Media I. Rayleigh and Love Waves from Buried Sources in a Multilayered Elastic Half-Space. *Bulletin of the Seismological Society of America*, 1964, 54(2), 627-679.

77. Haskell, N. A. Radiation Pattern of Surface Waves from Point Sources in a Multi-Layered Medium. *Bulletin of the Seismological Society of America*, 1964, 54(1), 377-393.

78. Yazdi, J. T., Valliappan, S., & Zhao, C. Analytical and Numerical Solutions for Wave Propagation in Water-Saturated Porous Layered Half-Space. *Soil Dynamics and Earthquake Engineering*, 1994, 13(4), 249-257.

79. Xu, B., Lu, J. F., & Wang, J. H. Dynamic Response of an Infinite Beam Overlying a Layered Poroelastic Half-Space to Moving Loads. *Journal of Sound and Vibration*, 2007, 306(1-2), 91-110.

80. Xu, B., Lu, J. F., & Wang, J. H. Dynamic Response of a Layered Water-Saturated Half Space to a Moving Load. *Computers and Geotechnics*, 2008, 35(1), 1-10.

81. Luco, J. E., & Apsel, R. J. On the Green's Functions for a Layered Half-Space. Part I. *Bulletin of the Seismological Society of America*, 1983, 73(4), 909-929.

82. Apsel, R. J., & Luco, J. E. On the Green's Functions for a Layered Half-Space. Part II. *Bulletin of the Seismological Society of America*, 1983, 73(4), 931-951.

83. Yun-Min, C., & Shi-Ming, W. A New Method to Solve Characteristic Equation of Rayleigh Wave in a Layered Soil. *Journal of Zhejiang University (Engineering Science)*, 1991, 25(1), 40-52.